



Met Office

Changes to the Met Office NWP System for Parallel Suite 20: Operational November 2008

Forecasting Research Technical Report
No. 553
11/4/2011

Authors: Malcolm E Brooks, Mike Bush, Brett
Candy, Samantha Pullen, Richard Renshaw,
Mike Thurlow



Document History

	Name	Date	Comment
Prepared by:	Malcolm E Brooks, Mike Bush, Brett Candy, Samantha Pullen, Richard Renshaw, Mike Thurlow	February 2011	Completed First Draft
Reviewed by:	David Walters	March 2011	Final Draft
Approved by:	Sean Milton	May 2011	Approved

Abstract

This report describes a significant upgrade to the Met Office Numerical Weather Prediction (NWP) suite, implemented on 25th November 2008. A package of changes to the forecast models, data assimilation system and satellite and surface observation processing systems was applied, as much as possible, consistently in all of the operational NWP models.

The main changes in the data assimilation system were efficiency improvements in all models, a revised set of covariance statistics and the use of a Northern Hemisphere snow analysis in the global model, and Cloud assimilation changes in the regional models. New satellite observations include the use of WindSat, increasing data volume of ATOVS observations, and changes to the processing of surface observations. The model physics package included a large number of changes to the surface properties and flux calculations, radiative transfer model, boundary layer scheme, cloud microphysics and aerosol emissions and parameterisation over Europe.

The various trial runs of the PS20 upgrade showed a significant improvement in forecast quality to both global/large scale indicators, and to the 'weather' based verification metrics used in the Local Area Models over the UK and Europe. These performance gains were delivered both during the parallel suite and in subsequent operational implementation.

1 Introduction

This note describes the changes to the Met Office Numerical Weather Prediction system that were implemented with Parallel Suite 20 (PS20). The suite ran, in parallel to the operational suite, from the beginning of October 2008 and was implemented operationally on 25th November 2008 as the following operational cycles:

Global Model	G49
North Atlantic European Model (NAE)	E21
UK 4km Model (UK4)	UK4.13
MOGREPS global ensemble	MOGREPS_G5
MOGREPS regional ensemble	MOGREPS_R5

Table 1: Operational cycle numbers for the changes implemented in Parallel Suite 20.

The changes implemented in PS20 were applied, as much as possible, as a consistent set of changes across all models. The focus of this document will be on the impact of these changes on the Global and North Atlantic and Europe (NAE) models, as in general the same changes were applied to 4km UK model (UK4), Crisis Area Models (CAMs) and MOGREPS ensemble forecasting system with similar effect.

2 Testing Strategy

Prior to the implementation of the changes in the Parallel Suite, the following tests were conducted, based on control trials with the scientific formulation as Global Model cycles G47 (PS18) or G48 (PS19):

2.1 Global Model

In order to test the impacts of each of the Model Physics changes independently most of the model changes were tested using a set 15 Case Study forecasts initiated from operational analyses covering the periods of Spring, Summer and Winter of 2006. The data assimilation and observations changes were tested individually using a set of 4D-VAR data assimilation trials were run at N320L50 resolution for 1 month periods starting on the 12th December 2007 and 1st June 2008. Based on the results of the tests of the individual components, a combined Data Assimilation (DA), Satellite Applications (SA) and Unified Model (UM) package was tested in the 4D-VAR trials.

2.2 NAE

Initial NAE testing consisted of running a number of independent sets of case studies. The 18 cases run in these tests included intense precipitation, showers in a northerly airstream, snow, gales, stratocumulus, fog, sub zero temperatures and cases where there were large errors in temperature and aerosol forecasts. The cases were chosen from the period starting on the 20th August 2007 and ending on the 23rd March 2008. The different suites tested many of the physics changes individually and others in packages (such as the boundary layer changes). Each suite was an incremental build on the previous so that each test became the control for the next one. This method has the advantage that interactions between the changes are tested (this would not be the case if each test was simply against the control) and the impact of each change is simply the difference between two incremental runs. However the disadvantage of this method is that it does not offer such a clean test of each individual change and any poor performing changes complicate the analysis of subsequent tests.

Analysis of the results led to the boundary layer and initial tests of a new prognostic cloud scheme being dropped from the NAE PS20 list of potential changes due to poor performance. The other changes were grouped into a conservative package of changes that were bug fixes or positive and various 'stretching' packages that included more ambitious changes.

These physics packages were then tested at half resolution (24km) with full 4D-VAR data assimilation and a 'conservative' DA package. Similarly, different DA packages were tested using one of the physics packages. Two periods were trialled, one being 16th December 2007 to 15th January 2008 and the other a real time trial which started on 6th August 2008 and finished on 21st September 2008. Finally, when the best physics and DA packages had been identified, they were trialled together for the Winter period with associated software version upgrades.

3 Description of Model Changes and Results from Individual Components

In this section we briefly describe the changes to the model and give an overview of their impact as individual changes rather than as a package of changes (as described in section 4).

3.1 Data Assimilation Changes

3.1.1 Code versions (A.Maycock, S.Oxley: Global/NAE/UK4/CAMs)

OPS and VAR were upgraded to stable versions 24.2.1 and 24.2.2 respectively.

3.1.2 Revised covariances (M.Thurlow: Global)

New covariances were introduced for the global atmospheric analysis. They were calculated by accumulating statistics from differences of T+6 and T+30 forecasts valid at the same time generated by a trial with the formulation of global model cycle G45 (PS16) covering the period 1st to the 31st January 2007. In addition to picking up a more recent model climatology (the set of covariances operational at G48 were produced in 2005 with a formulation similar to PS9) the new covariances were calculated at a resolution of ~55km (N216). By working with covariances at a higher resolution than the VAR grid at N108 we retain features and length scales that would otherwise have been lost with a native N108 set of covariances. This is more evident in the smaller scale control variables of unbalanced pressure and total water humidity than in the large scale stream function and velocity potential. There is evidence however that balance, as measured by the ratio of velocity potential to stream function, is slightly improved with the new covariances especially during Northern Hemisphere (NH) summer.

The pre-PS20 operational covariances were produced for an NH summer period whereas the new covariances are for an NH winter. This change of season moves the hemisphere of greater variance (and therefore smaller observation weight) from south to north. The effect on the tropics is smaller but shows a slight increase in variance and therefore decrease in observation weight.

Overall there is a general reduction in the size of the analysis increments passed on to the IAU as shown in Figure 1. The largest change is seen in the size of the total water increments in the stratosphere where the maximum magnitude is reduced by up to two orders of magnitude but unfortunately the impact of this is somewhat ameliorated by the stratospheric readjustment of humidity which takes place in the IAU. The most significant exception to the general reduction is seen in the theta increment which has a maximum RMS and maximum value larger than that produced by the current (ie pre-PS20) covariances and shifted down a level to model level 47. For both sets of covariances, this peak is associated with high theta value regions in the winter (greater variance) hemisphere when the season matches that of the covariances. For the current covariances this has caused occasional operational UM stability problems in the Southern Hemisphere (SH) which have been countered by limiting the maximum size of the theta increments applied by the IAU. In principle this could occur with the new covariances in the NH and so the IAU theta increment limiter remains enabled.

For consistency the new covariances are also used in the 3D-Var screen analysis. The impact of the change on most variables is slight with the most significant differences being a small warming at the surface and a marginally better fit to surface winds.

In trials the net effect on global NWP index (see Section 4.2) was positive with verification against analyses performing exceptionally well (+1.3 in NH summer and +2.3 in NH winter) though verification against observations was less positive (+0.3 in NH summer and -0.8 in NH winter). The poor NH

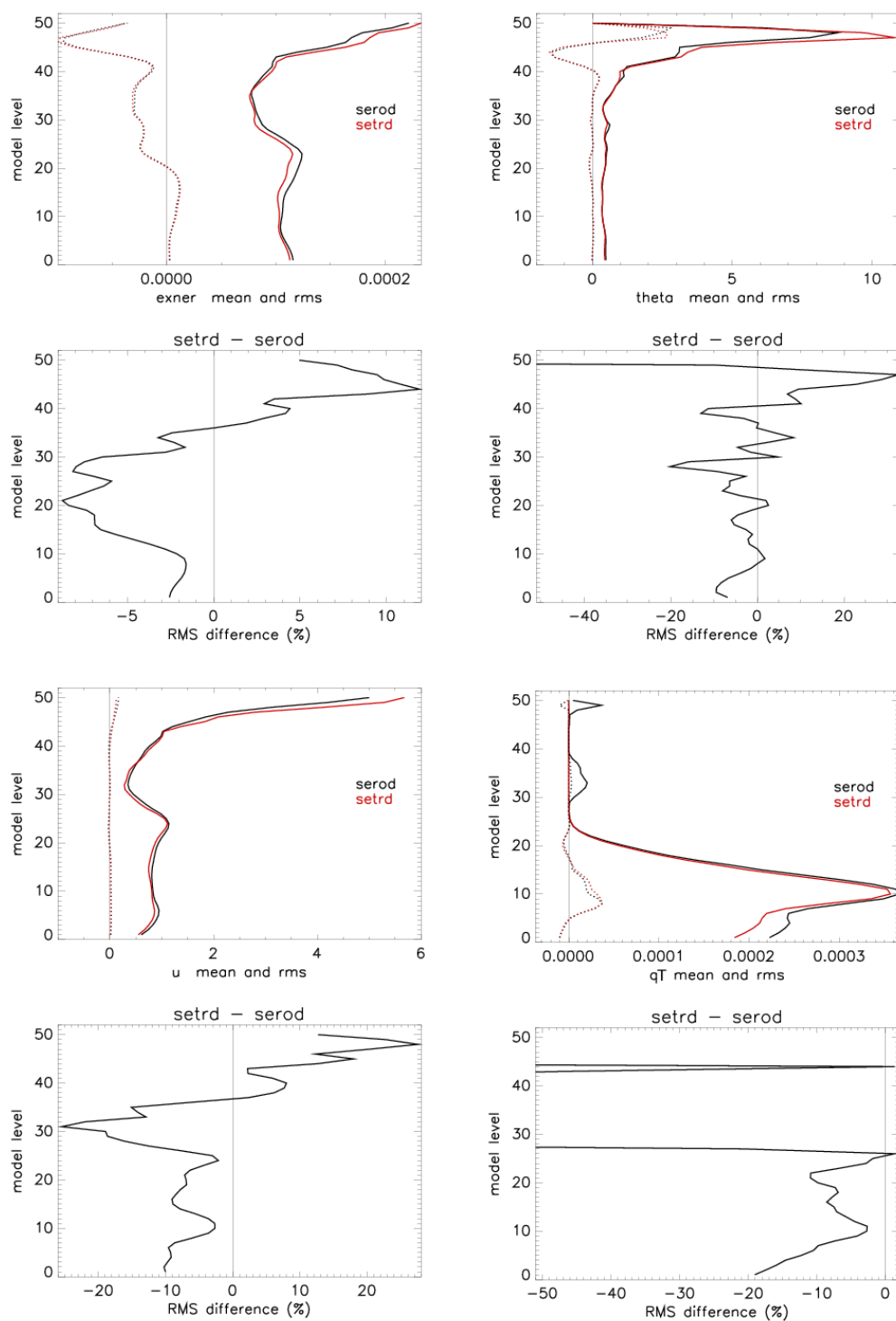


Figure 1: Average mean and RMS increments of exner pressure, potential temperature, u component of wind and total water content for an NH winter control and trial together with the difference in RMS between the two. serod is a G48 (PS19) N320 control using current operational covariances; setrd is a copy of serod with the covariances replaced by the N216 PS20 set.

winter value is not reflected in large forecast RMS errors (see Figure 2) but a consequence of small persistence errors distorting the skill score and so may not be a typical NH winter feature.

SETRDVSEEROD: NEW(N216) V OPER COVSTATS (PS19) (DEC 2007) SETRDVSEEROD: NEW(N216) V OPER COVSTATS (PS19) (DEC 2007)

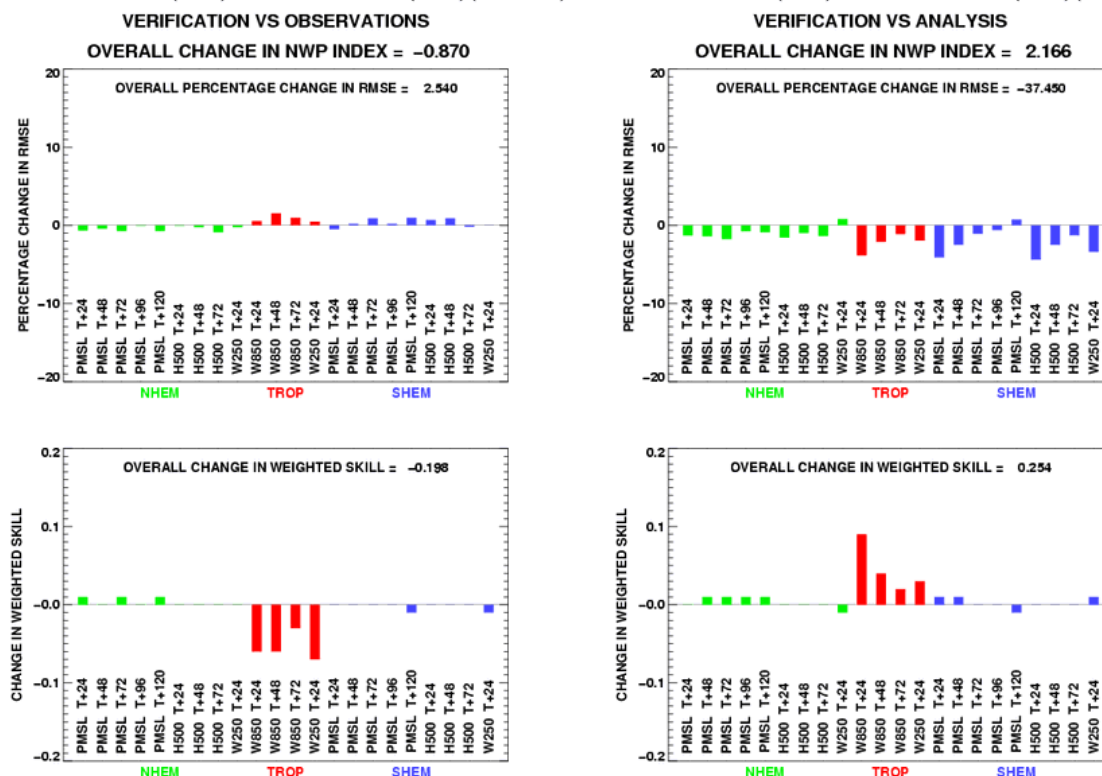


Figure 2: Changes to RMS error for fields in the global NWP index for an NH winter trial. The control is a G48 (PS19) N320 trial using current operational covariances. The trial differs from the control only in the replacement of the covariances with the new N216 PS20 set.

As a final note a further benefit of using covariances at N216 within an N108 VAR configuration is that it will allow future increases to the resolution of VAR to be evaluated separately from any change of covariance that would have otherwise needed to have been made.

3.1.3 Inclusion of ice in moisture incrementing operator (M. Sharpe: Global/NAE)

This change implements a change to both VAR and UM codes to both analyse and initialise frozen cloud thereby extending the existing capability for liquid cloud. All observation types that make use of any moisture variable, liquid or frozen cloud fraction, or bulk cloud fraction in their OPS operators are affected. The impact of the change is neutral at present but should be of greater importance as new observation types are introduced in the future.

3.1.4 VAR PF GCR efficiency improvements (W.Grey, T.Payne: Global/NAE)

Solving the Helmholtz equation every timestep of the PF model for every minimisation iteration is a major contribution to the cost of running 4D-Var. However iterating the GCR Helmholtz solver to full convergence in the early stages of minimisation of the penalty function is wasted effort as we are then still some way from the final analysis. This change limits the number of GCR iterations each PF model timestep in the early stages of the minimisation to a smaller number than is required for full convergence of the solver. The limit is applied for a specified number of iterations from the start of the minimisation after which the GCR solver reverts to normal full convergence behaviour. The overall effect is to reduce the run time by about 20% with no impact on the quality of the final analysis. This change is applied only to main runs.

3.1.5 Improved VAR first guess in update runs (M.Thurlow, G.Inverarity: Global/NAE)

This change reduces the time required to run VAR in update runs by using the main run analysis (in the form of a vector of VAR control variables) as the first guess for the minimisation. A reduction of up to 40% in the number of iterations and therefore run time is found with a small improvement in the quality of the update run analysis as measured by fits to analyses and to a lesser extent observations.

To allow for the possibility that the control vector is not produced or saved by the main run, suite task filtering is used to fall back to a normal VAR analysis if one cannot be found.

3.1.6 Northern Hemisphere snow analysis (S. Pullen, G. Rooney, C. Jones: Global)

This change introduces the first observational snow information into the global model on a daily basis (Pullen *et al.* (2008)). A snow analysis has been developed using the National Environmental Satellite Data and Information Service (NESDIS) Interactive Multisensor Snow and Ice Mapping System (IMS) snow cover product (Helfrich *et al.* (2007)). This is a daily Northern Hemisphere (NH) snow map at 4 km resolution, derived primarily from satellite imagery. The binary snow cover data (fully covered (1) or no snow (0)) is converted to a fractional snow cover at model resolution and then compared with the model background snow amount, in terms of snow presence. Where there is disagreement as to the presence of snow, snow is removed from or added to the model snow field to better match the observational data. The amount of snow to be added is determined using an empirical relationship from Essery *et al.* (1999) between fractional cover and snow water equivalent, up to a maximum of 10 kgm^{-2} .

Trials run over December 2006 and March-May 2007 yielded neutral results in terms of the NWP index but there is some evidence of improvements in surface and low level temperature and relative humidity forecasts, especially where snow is predominantly removed by the snow analysis.

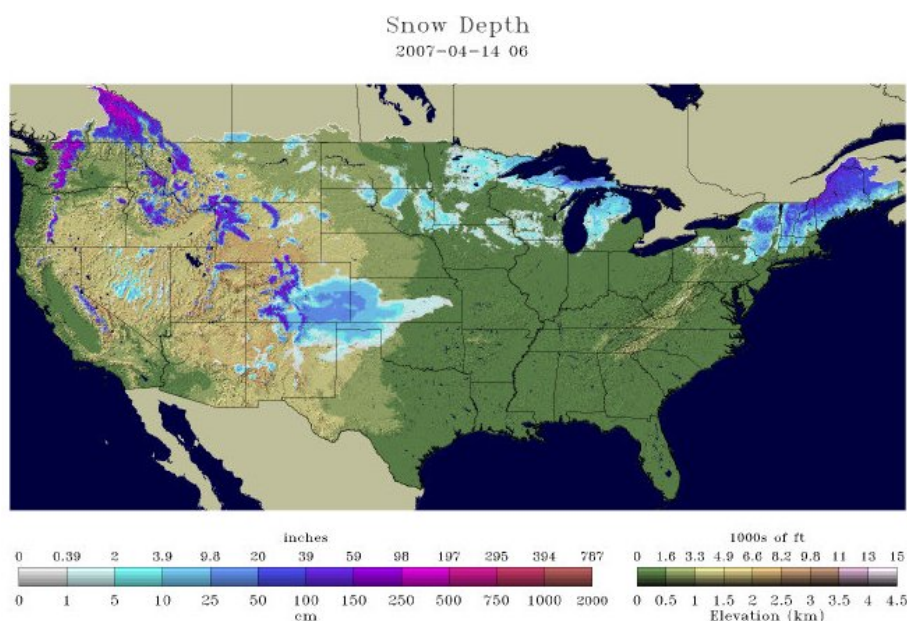


Figure 3: An example snow depth from the National Operational Hydrological Remote Sensing Center (NOHRSC).

The snow analyses verify well in qualitative terms against other observational and analysed snow cover products, in most cases improving the model representation with excess snow being removed from the snow accumulation period (December) and snow reinstated into the model during the melting/ablation period (March-May) where the model had removed it too quickly. A typical example is shown in Figures 3 and 4. An independent snow analysis in Figure 3 shows widespread but scattered and shallow snow cover over much of the Northern USA. The model background, in Figure 4, has already melted most of this snow which the snow analysis then adds back into the model, giving much better agreement with Figure 3. Quantitative verification against SYNOP reports of snow-covered ground in Europe shows the snow analysis increases the proportion of model gridpoints where the snow cover agrees with the SYNOP reports of snow.

3.1.7 Assimilation of MOPS cloud data in VAR rather than AC scheme (R. Renshaw: NAE/UK4)

The UK regional models have for many years assimilated cloud fraction through the AC (Analysis Correction) scheme within the UM, alongside latent heat nudging for precipitation. The long-term aim is to incorporate both of these into the main variational data assimilation system (VAR), allowing the removal of old code from the UM, and a single integrated assimilation system for all observation types. In PS20 the cloud data is assimilated through VAR. Extensive trialling has shown a continued positive impact overall from cloud assimilation but relatively little difference between cloud assimilation in VAR and cloud assimilation in the AC scheme. This change was made to meet our long-term aims and to

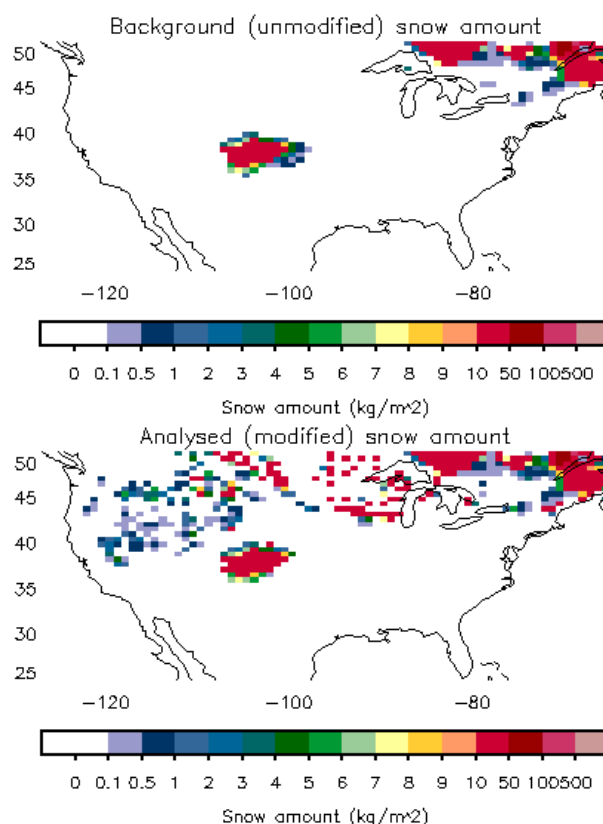


Figure 4: Snow amount over the USA for 14th April 2007, before and after the use of the snow analysis.

allow development using other sources of cloud data.

3.1.8 Switch source of MOPS cloud from NIMROD to EUROPP (NAE) and UKPP (UK4)

The NIMROD nowcasting system provided the NAE and UK4 with cloud fractions at 15km resolution over the UK area derived from satellite imagery and surface reports. NIMROD was switched off shortly after PS20, but the cloud data continued to be provided by the NIMROD replacements EUROPP (North-Western Europe Post-Processing, 5km) and UKPP (2km). Final testing was not possible prior to PS20 but the higher resolution and, for the NAE, increased coverage was thought to give some potential benefit to the cloud assimilation.

3.1.9 Assimilation of SEVIRI clear-sky radiances (G.Kelly: NAE/UK4)

The Spinning Enhanced Visible and Infrared Imager (SEVIRI) instrument on the Meteosat Second Generation (MSG) satellite provides regular high-resolution imagery at several wavelengths sensitive to temperature and water vapour. This data can be assimilated in the same way as Advanced TIROS

Operational Vertical Sounder (ATOVS) and other radiances. Quality control checks reject cloud-contaminated pixels. Trialling showed a small but positive impact.

3.1.10 Assimilation of extra GRAS ground-based radio occultation data (M.Rennie: NAE)

This was applied to the NAE for consistency with the Global model, which has used these extra observations since G48 (PS19) in July 2008. This change has a minimal computational cost and was not expected to provide any significant impact.

3.2 Satellite and Observations Changes

3.2.1 Introduction of WindSat (S.Keogh, B.Candy: Global)

Wind Vector retrievals from the WindSat polarimetric radiometer (Bettenhausen *et al.* (2006)) have been available at the Met Office in near real time since autumn 2006. This instrument is onboard the Coriolis research satellite and is operated by the US Navy. These data arrive at the Met Office in binary files with a format specific to the US and are converted to BUFR and sent to the MetDB via WindSat PrePare, a set of programs designed within Satellite Applications for this purpose. Although the Coriolis satellite is not part of a standard operational series data reliability is good - only four outages in the twelve month period from November 2007. The wind vectors have a directional ambiguity and so are assimilated using the cost function developed for scatterometer observation types. Pre operational impact studies showed that when the WindSat data is assimilated on top of a control that contains the existing scatterometer network a neutral impact is observed, although the positioning errors of two tropical cyclones were improved (3% overall). However earlier impact studies (Candy *et al.* (2009)) have shown comparable impact to the QuikScat scatterometer on top of a control run in which no satellite surface wind data was used. Figure 5 shows the coverage of 24 hours of WindSat data after screening for low wind speed regions and rain in the field of view.

3.2.2 ATOVS data from RARS stations in the Southern Ocean (B. Candy : Global/CAMs)

For several years now ATOVS data from Regional ATOVS Retransmission (RARS) networks have been used to supplement the global ATOVS data arriving from NESDIS/EUMETSAT. The RARS data has been shown to be more timely and can fill in missing data which does not arrive in time to make the main run cutoffs (Candy *et al.* (2008)). The RARS network has recently expanded to include data from South America / Antarctic coast and in PS20 data from Cordoba, Base Marambio and Davis are used for the first time. Figure 6 shows the locations of RARS stations used in the global model.

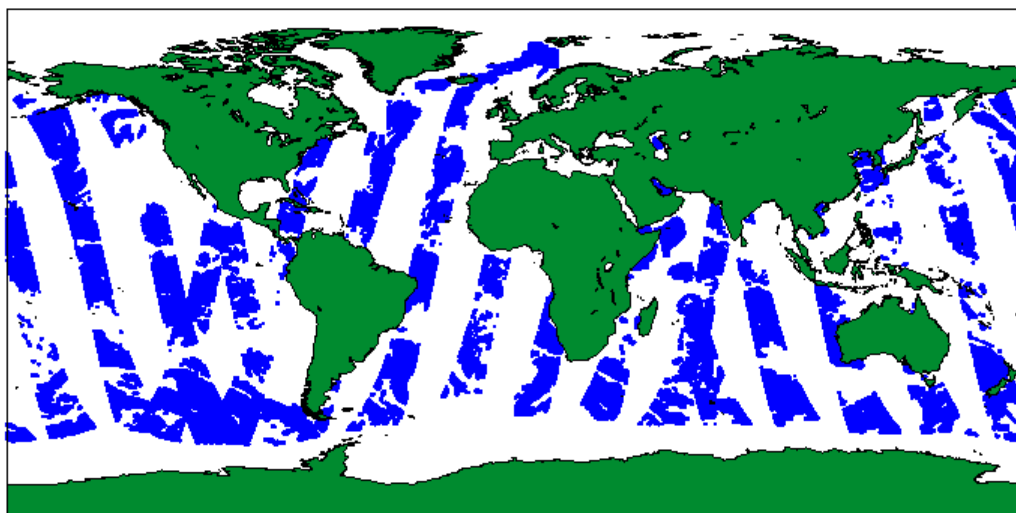


Figure 5: Data coverage from 24 hours of WindSat data after quality control is applied.

3.2.3 Minor surface data processing changes (B.Ingleby: Global/NAE/UK4/CAMs)

The observation error has been decreased for automated marine observations and increased for manual ship reports. This change has an immediate impact on forecasts but two further diagnostic changes were included for future use. Firstly, extra associated data were stored in the MetDB tidying up RH and wind speed corrections, allowing for upcoming changes to pressure processing, and adding precipitation, cloud, radiation, soil and boundary layer fields for use in diagnostic studies. Note that the radiation field is not time interpolated and is available only at T+6 and that the precipitation data is flagged as missing data for the time being. Secondly, mobile synops (MOBSYN) were included for monitoring purposes prior to future trialling of their assimilation.

3.3 Forecast Model: Land Surface

3.3.1 Fractional snow cover for sublimation and melting aka 'Tibetan snow mod' (G.Rooney: Global/NAE/CAMs)

For low snow amounts, this implements a basic representation of the distribution of snow across a grid box by splitting the surface into a snow covered and snow free area. As the effect of this change is limited to areas with low snow cover, the impact is minimal, however within these area the new treatment is more physically realistic than the current scheme where very small amounts of snow are spread across the entire grid box which is thought to cause numerical instabilities as the snow melts.

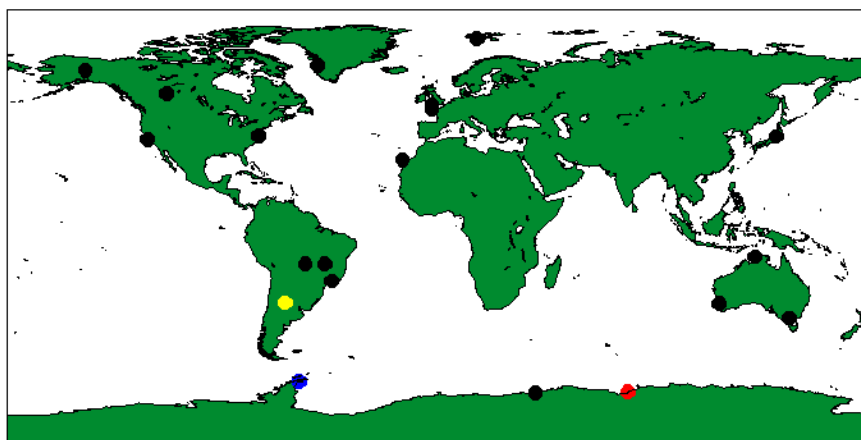


Figure 6: Locations of RARS ground stations used to supplement ATOVS global data. Key: black denotes existing stations, yellow Cordoba, blue Marambio and red Davis.

3.3.2 CLASSIC Albedos (M.Brooks, Clive Jones: Global/NAE/UK4/CAMs)

This change uses data provided by the Climate and Land-Surface Systems Interaction Centre (CLASSIC) and described by Houldcroft *et al.* (2008) which uses MODIS data to derive a much more accurate specification of the albedo of the Met Office Surface Exchange Scheme (MOSES) vegetated tiles (see Table 2) and of the underlying bare soil. An initial evaluation of the CLASSIC data by Brooks and Jones (2007) shows that the errors in surface albedos are significantly reduced and that, in the absence of a dedicated cropland tile in MOSES, the best results are obtained by using the observed albedo of crops for our C3 grass tile. Figure 7a) shows the annual snow-free albedos from a MODIS climatology from Moody *et al.* (2005). Panel b) shows the error in G41/PS12 which was the first cycle to use the current (IGBP) land use dataset - with a set value of the soil albedo over the Sahara. Panel c) shows G44/PS15 which included a seasonally varying Leaf Area Index (LAI) of vegetation and the bare soil albedo was modified towards the Moody *et al.* (2005) climatology, weighted according to the bare soil fraction in the land use data. Meanwhile panel d) shows the error for G49/PS20 which uses the CLASSIC albedo values for both the bare soil and vegetated tiles.

	Broadleaf Trees	Needleleaf Trees	C3 Grass	C4 Grass	Shrubs
Pre-PS20	0.1	0.1	0.2	0.2	0.2
PS20	0.143	0.088	0.192	0.159	0.115

Table 2: Fully vegetated snow free albedos for the MOSES plant functional types.

Figure 7 clearly shows the reduction in the albedo errors from PS12 to the PS20 configuration, reducing the bias from +0.019 to only -0.00028 and halving the RMS errors. It is likely that the CLASSIC albedos are the best albedos that can be produced by the current method which has fixed

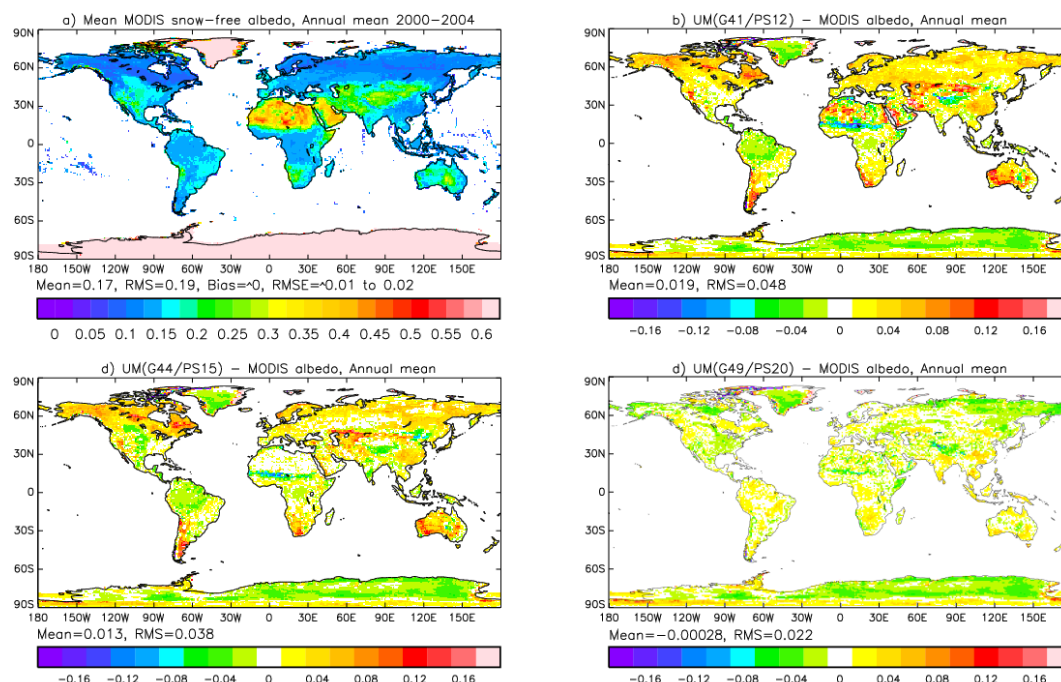


Figure 7: a) Annual mean snow free albedo from the MODIS climatology of Moody *et al.* (2005), and (b,c,d) the mean error of the albedo for the Met Office global model for three different configurations. Mean and RMS statistics are only calculated over un-glaciated land points.

values of the albedos of the vegetation types (for high LAI). Tests in the NAE showed the CLASSIC albedo improved forecasts of near surface temperature, cloud and visibility, while in the global model the use of the CLASSIC albedos had a comparatively small impact on large scale metrics used to measure model performance.

Unfortunately the Winter data assimilation trials of the combined DA/SA/UM package experienced a prolonged period of model instability. The instabilities were occurring high in the Andes, at an altitude of $\sim 3500\text{m}$ where the land use is bare soil with only patchy and intermittent snow cover. These points were being heated by strong solar insolation causing a deep boundary layer to develop which was being capped by the hard-wired maximum number of boundary layer levels (which is at a lower altitude over high orography where the bottom model levels are compressed). The artificial capping of the boundary layer eventually led to unphysically strong explosive convection which caused the model to fail.

This is not a new problem - the operational global model at the time also experienced a period of instability during the period. The operational log files showed that were unusually high iteration counts in the dynamics solver and the 14th December 2007 main midday forecast failed and required a shorter timestep. However the introduction of the CLASSIC bare soil albedos (bsa) exacerbated this problem as, in this region, they are darker than the previous albedos (~ 0.15 as opposed to

~0.25). Trials of several different variants of the package were run to investigate the problem and these typically failed 6 or 7 times during the first week. An interim fix was implemented whereby the *bsa* was modified based on the model orography with the CLASSIC *bsa* used below 2500m and scaling linearly to the old values used above 3000m.

3.3.3 Surface Emissivity (consistent with NAE) (M.Bush, M.Brooks: Global/CAMs)

By changing the LW emissivity from 1.0 to 0.97 this brings the global and CAM models closer to observations (which range from ~0.8 to ~0.99) and is also consistent with the NAE. The impact of this change is difficult to determine as it was tested alongside the CLASSIC albedos, which showed a neutral performance.

3.3.4 Canopy Radiation (I.Dharssi: Global/CAMs)

Implements a multi-layer approach for both radiation interception (2-stream approach of Sellers *et al.* (1992)) and canopy photosynthesis (Mercado *et al.* (2007)), as opposed to the previous single 'big-leaf' approximation. In previous VAR trials for G48 (PS19) this was found to this reduced the Northern Hemisphere summer warm bias by ~ 0.2K and gave neutral NWP index impact in both Summer 2006 and Summer 2007.

3.4 Forecast Model: Radiation

The following radiation changes constitute a significant set of corrections. An example of the impact of these changes to the large scale global model fields is shown in Figure 8 and to the NAE model cloud cover in Figure 9.

3.4.1 Updated CO2 and trace gases (M.Brooks, J.Manners: Global/NAE/CAMs)

The concentrations of CO2 and other trace gases were updated in all of the NWP models, to account for the continued increases in the concentration of these gases, to values in Table 3. Figure 8 shows that this change slightly warms the troposphere, particularly at lower levels, and cools the stratosphere. The biases in Pressure at mean sea level (P_{msl}) and 500hPa height (H_{500}) are slightly improved while the winds are unaffected on the 5 day timescale which is consistent with the homogeneous warming applied by this change (not shown). It should also be noted that the concentrations of these gases were being correctly represented in the Met Office climate models.

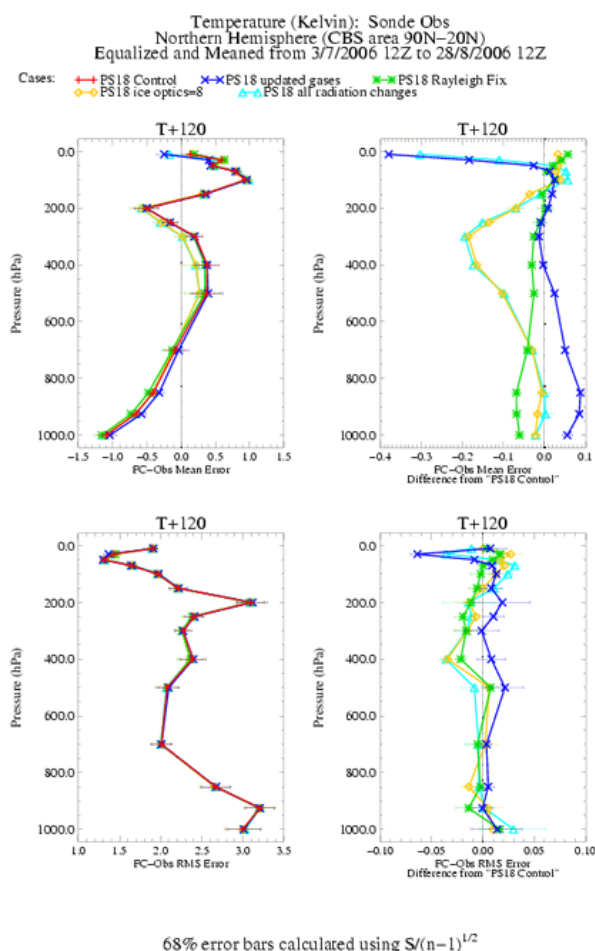


Figure 8: Impact of radiation changes to the Northern Hemisphere temperature profile compared against Sonde observations in global model case studies with Model Cycle G47 (PS18) taken as the control. The figure in the top left shows the mean bias and the figure in the bottom left shows the RMS error. The figures on the right hand side show the changes in the the bias/RMS relative to the control run for each of the experiments.

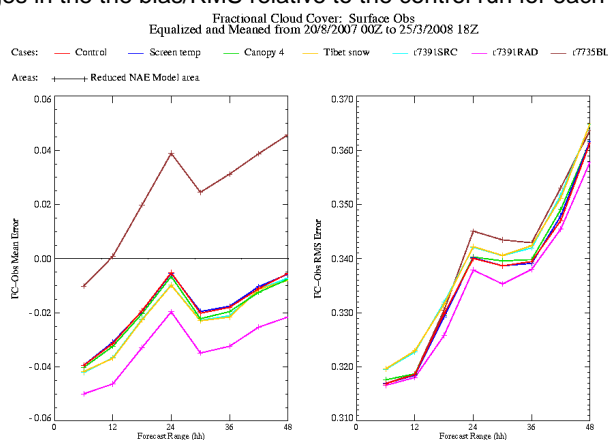


Figure 9: Impact of radiation changes (purple coloured line) on NAE cloud cover bias (left panel) and RMSE (right panel). The radiation changes reduce the amount of cloud and improve the RMSE.

Gas	CO ₂	CH ₄	N ₂ O	CFC-11	CFC-12
MMR	5.844e ⁻⁴	9.850e ⁻⁷	4.880e ⁻⁷	1.164e ⁻⁹	2.253e ⁻⁹

Table 3: Updated values for trace gas mass mixing ratios.

3.4.2 Rayleigh Scattering Bugfix (J.Haywood, B.Johnson, M.Brooks: Global/NAE/UK4/CAMs)

A long standing error was identified in code which pre-processes the Rayleigh scattering properties of dry air for the so-called spectral files used by the forecast model. Correcting this error slightly increases the scattering of solar radiation in clear skies but has a minimal impact on the quality of the forecast, causing the small tropospheric cooling in Figure 8 which cancels out much of the effect of the updated gases in 3.4.1.

3.4.3 Ice Optical Properties. (J. Edwards, A.Baran, M.Brooks: Global/NAE/CAMs)

This change implements a more recent and improved treatment of the ice optical properties as described in Edwards *et al.* (2007), where the ice optical properties are treated as an ensemble of different non-spherical ice particles. This parameterisation has been used in Met Office climate models for since HadAM3 (Pope *et al.* (2000)). The main impact of this change in the global model is shown in Figure 8 where it reduces the warm temperature bias in the upper troposphere in the Summer Hemisphere from a peak of +0.5 to +0.3. It also induces a similar beneficial impact in the tropics (not shown) and reinforces a smaller cool bias in the upper troposphere in the Winter Hemisphere.

3.4.4 Correction to parameterisation of extinction by ice crystals. (M.Bush, J.Manners: NAE)

The long-wave extinction due to ice crystals was significantly overestimated in the NAE, due to a long-standing error in the parameterisation of the ice optical properties it employed. This is corrected so that the NAE uses the same parameterisation of extinction as the other Met Office atmospheric models.

3.4.5 HadGEM spectral files (D. Walters: CAMs)

Here we replace the Meso2 spectral files in the CAM with the HadGEM spectral files used in the operational Global Model. This allows more accurate but more expensive radiation calculations, which previous tests have shown to improve temperature profiles.

3.4.6 38 Ozone levels (D. Walters: CAMs)

The CAMs still uses an ozone ancillary defined on only the top 11 of their 38 vertical levels, whilst all other operational models use climatologies on every model level. This was not included in previous upgrades as it made the near-surface cold bias worse, however it is now being included as the CAM now has a near-surface warm bias.

3.5 Forecast Model: Microphysics

The following microphysics changes are physics upgrades based, for the most part, on radar/lidar observations of clouds from the CloudNET project (Illingworth *et al.* (2007)). The impact of these changes to the temperature profile in the global model is shown in Figure 10. The impact on P_{msl} and winds was minimal, apart from tests of an early implementation of the water droplet fallspeed changes described Abel and Shipway (2007), which are mentioned in Figure 8, but were not included in PS20.

3.5.1 3D Microphysics (D.Wilson, J.Petch, J.Wilkinson, C.Morcrette: Global/NAE/CAMs)

The 3D microphysics scheme is scientifically very similar to the current 3C scheme but has been rewritten to allow more opportunities for scientific development. The most important of these is the use of droplet settling (see 3.5.4) and compatibility with the new PC2 cloud scheme which is intended for future upgrades. Although the 3C and 3D schemes are very similar it has been found that the structure used to implement the falling and melting of ice in the 2 schemes differs sufficiently that using the 3D scheme has a larger impact on the forecast than would be expected purely from rewriting the code. Figure 10 shows the 3D microphysics scheme causes a cooling through the upper troposphere, although the magnitude of the change is relatively small compared to the Radiation changes in Figure 8.

3.5.2 Brown & Francis Ice Particle Densities (D.Wilson, J.Petch, J.Wilkinson, C.Morcrette: Global/NAE/CAMs/UK4)

There is evidence from radar data from CloudNET that the density relationship used within the UM is too large, causing thick ice cloud to develop in the model. This new relationship gives a more realistic ice particle size to density relationship from Brown and Francis (1995).

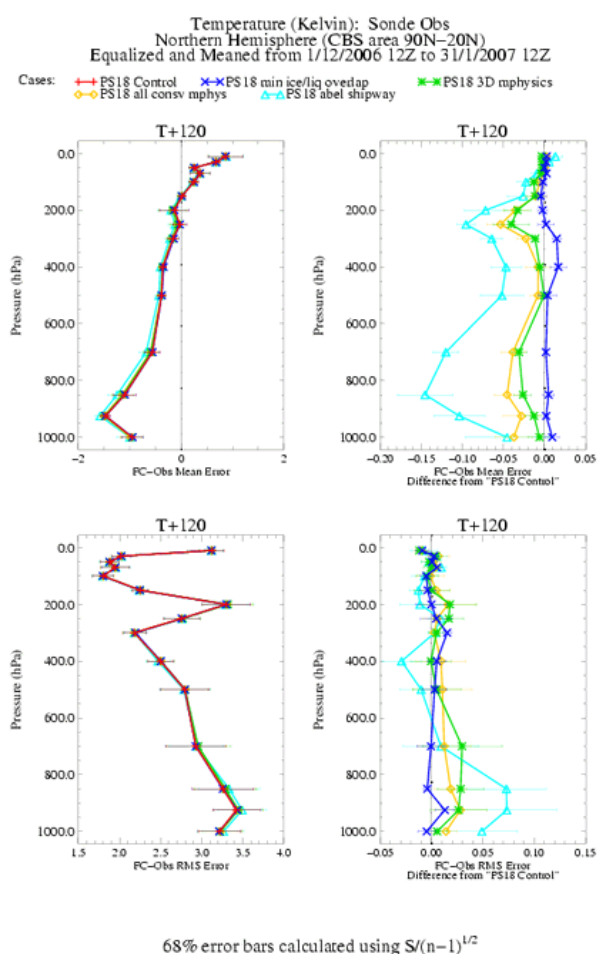


Figure 10: Impact of microphysics changes to the Northern Hemisphere temperature profile compared against Sonde observations in global model case studies with Model Cycle G47 (PS18) taken as the control. The figure in the top left shows the mean bias and the figure in the bottom left shows the RMS error. The figures on the right hand side show the changes in the the bias/RMS relative to the control run for each of the experiments. the 'all consrv mphys' experiment contains all of the changes listed in 3.5, while the Able and Shipway line was part of a 'stretching' package of model physics upgrades which was not included.

3.5.3 Mitchells 2nd Re-X Relationship (D.Wilson, J.Petch, J.Wilkinson, C.Morcrette: Global/NAE/CAMs/UK4)

This change applies the a new relationship from Mitchell (1996) between the effective radius (R_e) of ice particles and the Best number, X , which is used in the calculation of ice terminal velocities. It is required in conjunction with the Brown & Francis densities so that the new ice particle densities produce sensible fall speeds.

3.5.4 Droplet Settling (D.Wilson, A.Lock, J.Petch, J.Wilkinson, C.Morcrette: Global/NAE/CAMs/UK4)

Droplet settling allows the cloud droplets to slowly fall from clouds with typical velocities of $\sim 1\text{ms}^{-1}$. This has very little effect on cloud or surface rain rates, but has been shown to improve forecasting the evolution of fog, with a particular example being the Christmas Fog of 2006. The impact of the Brown & Francis Ice Particle Densities, the Mitchells 2nd Re-X Relationship and Droplet settling to the large scale global model is small, as shown by the difference between the 3D and the 'all conv mphys' lines in Figure 10.

3.5.5 Minimum Overlap Between Ice and Liquid clouds (D.Wilson, J.Petch, J.Wilkinson, C.Morcrette: Global/NAE/CAMs/UK4)

This change should allow supercooled liquid water clouds to persist for longer in the model by changing overlap between ice and liquid clouds (in the same grid box) so that the ice clouds do not immediately destroy the water droplets by preferential condensation onto the ice particles. The CloudNET observations show that supercooled liquid water clouds are far more common in reality than they are forecast in our models and clouds such as a glaciating altocumulus can be easily observed to have a minimum overlap between the ice and liquid clouds. Figure 10 shows that this change has a minimal impact on the forecast fields, and it also showed no significant impact in the NAE.

3.5.6 MURK Link to Autoconversion (J.Wilkinson: NAE/UK4)

Autoconversion from cloud droplets to drizzle uses some assumption of cloud droplet size. At present this is a fixed value for land and another fixed value for sea, resulting in a unrealistic land-sea split in drizzle rates. Linking MURK aerosol (see section 3.6) to autoconversion rates removes this tendency and should produce more realistic drizzle patterns. There is also evidence that this acts to reduce some of the more spurious drizzle that occurs in cloudy anticyclonic conditions (not shown).

3.6 Forecast Model: 'MURK' Aerosol changes

The Met Office local area models over the UK and Europe use a single prognostic aerosol species, named murk, to represent the impact of the aerosol and humidity on visibility, in order to improve the benefit from the assimilation of visibility observations (Clark *et al.*, 2008).

3.6.1 Improved MURK source dataset (M.Athanassiadou, P.Agnew, M.Bush: NAE/UK4)

An improved MURK emissions dataset was created from the GEMS-TNO emissions (5km x 5km) and EMEP (50km x 50km) together with emissions from shipping and a nominal value for sea salt. Over the U.K where stack heights from point sources are known, emissions from grid points corresponding to elevated point sources have been moved from the surface to the appropriate model level. For the UK4, sources originally at level 1 have been split evenly between levels 1 and 2 to avoid trapping aerosols in the bottom 5m in very stable conditions.

3.6.2 MURK parameterisation changes (M.Bush, J.Haywood: NAE/UK4)

A set of improvements were applied to the mode radius, number density and activation parameter (hygroscopic growth) of the MURK aerosol, as described by Haywood *et al.* (2008).

3.7 Forecast Model: Technical Changes

3.7.1 Upgrade to UM7.1 (All Models)

To simplify the process of porting of the operational models to the new IBM supercomputer all models were upgraded to use the Met Office Unified Model (MetUM) vn7.1 code. Only minimal code changes were allowed on top of the lodged code at 7.1, such as alterations to parameter settings and essential fixes. The tighter control of the MetUM code has been subsequently enforced, with all changes to the operational models since PS20 being either part of the latest release of the MetUM, or accepted for the subsequent release. This entails the change going through an internal scientific as well as technical peer review process and integration testing, before the change is lodged into the code-base for the next MetUM release.

3.7.2 LBC Formulation Part 1- technical change to use new structure (P.Lean, M.Bush, T.Davies: NAE/CAMs/UK4)

A more accurate lateral boundary formulation is implemented which results in a reduced solver iteration count and consequently a reduced runtime. In addition, these changes prepare the LBC code for the use of a different structure which produces smaller LBC files. The new LBC file structure will not actually be implemented at this stage.

3.7.3 T^* on all tiles (M.Bush, G.Rooney: NAE)

This change switches on an option for performing the calculation of the surface/skin temperature (T^*) on all surface tiles (except land ice) even when some tile fractions are zero. This will help the site specific forecasts (SSPS) deal with the potential application of urban - rural land-use fraction adjustment. The observing sites at Dyce, for example, currently has no C3 grass tile temperature while Benson has no urban tile temperature etc.

4 Performance of the Parallel Suite and Trials Testing Combined Package

4.1 Large scale global circulation

As a first indication of the performance of the global model in forecasting the large scale global circulation, Figure 11 shows the forecast performance, compared against all available surface observations, for Northern Hemisphere Pressure (at mean sea level, P_{msl}) during the December 2007 and June 2008 trials, against forecast lead time. Broadly speaking the P_{msl} biases are left unchanged, while there a significant reductions in the RMS errors, especially at longer lead times, in both of the trials with the final setup. The winter trial without the new covariances (described in Section 3.1.2) shows only a very slight reduction in the P_{msl} RMS error, highlighting the importance of using the best statistics in the data assimilation system. The maps of the RMS errors of P_{msl} , shown for the winter trial in Figure 12, show the largest reduction in P_{msl} RMS error the storm track regions of the North Atlantic and Pacific. Performance in the Southern Ocean is mixed with a large areas of both improvement and degradation.

As an indicator of the performance of the mid-level circulation and low-level thermal structure, similar plots are shown in Figure 13 comparing the forecast geopotential height of the 500hPa surface (H_{500}) against all available sonde obs in the Northern Hemisphere. During Winter, a negative H_{500} bias is worsened, while during Summer a positive H_{500} bias of similar magnitude is corrected, while the RMS errors are reduced significantly, especially at long forecast lead times, in both of the trials with the final setup. As with the P_{msl} , the RMS error maps, against analyses for T+144, shown in Figure 14 show that the reduction in RMS error mainly in the North Atlantic and Pacific storm track regions, while the Southern Ocean shows large regions of both improvement and degradation.

The disparity between the Winter and Summer biases in H_{500} is worth further examination, and the biases in the Temperature profiles against Sonde observations is shown in Figure 15. The PS20 physics package acts to cool the troposphere in both the both Summer and Winter trials, which acts

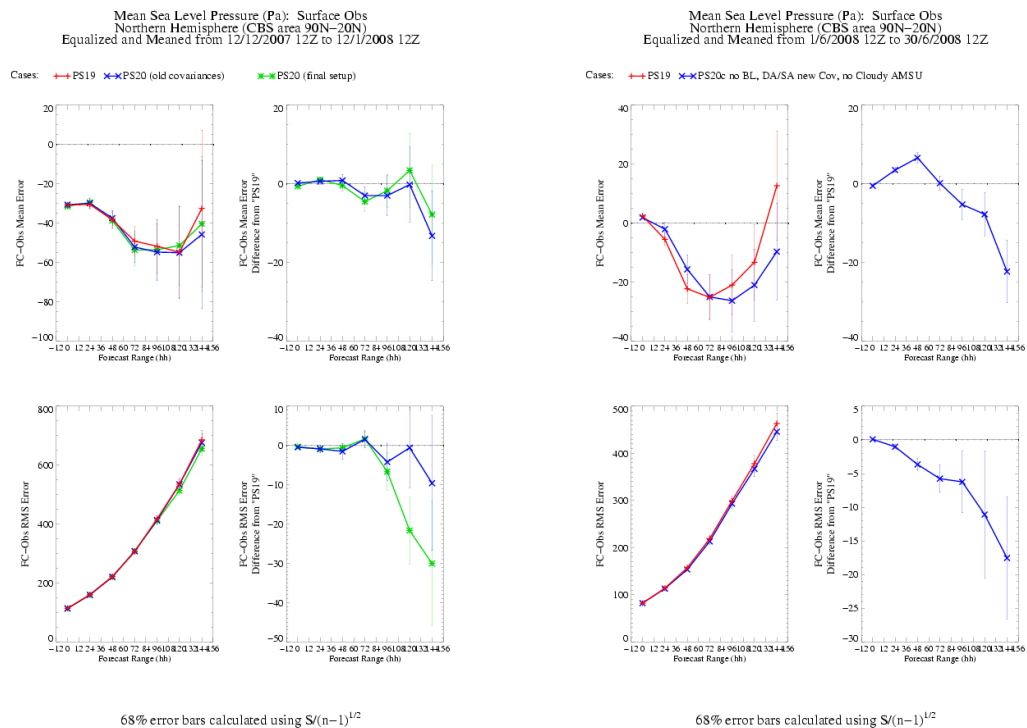


Figure 11: Impact of radiation changes to the G49 (PS20) package on Northern Hemisphere (NH) Pressure at mean sea level (P_{msl}) forecasts for the December 2007 and June 2008 periods, verified against surface observations and compared to the previous G48 (PS19) model. The December trial also includes a version of the package without the new covariances described in Section 3.1.2.

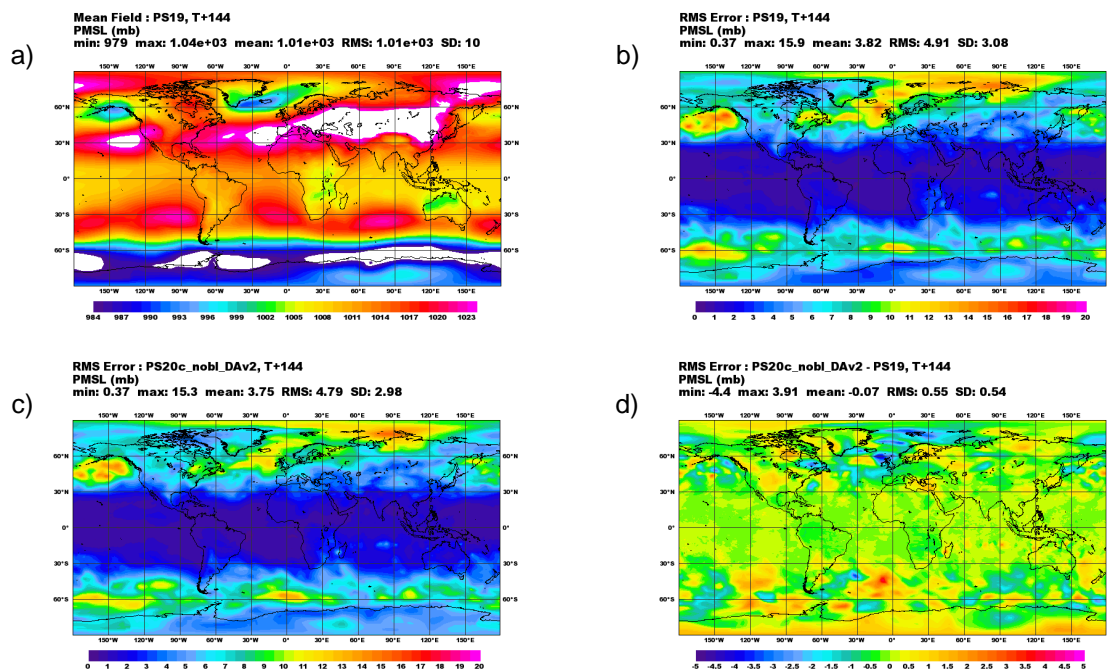


Figure 12: a) Mean P_{msl} analyses (which verify at the same times as panels b-d), during the December Trial from the PS19 control analyses, for reference against the forecast RMS errors, at T+144, of the PS19 (b) and PS20 (c) trials, and their differences (d).

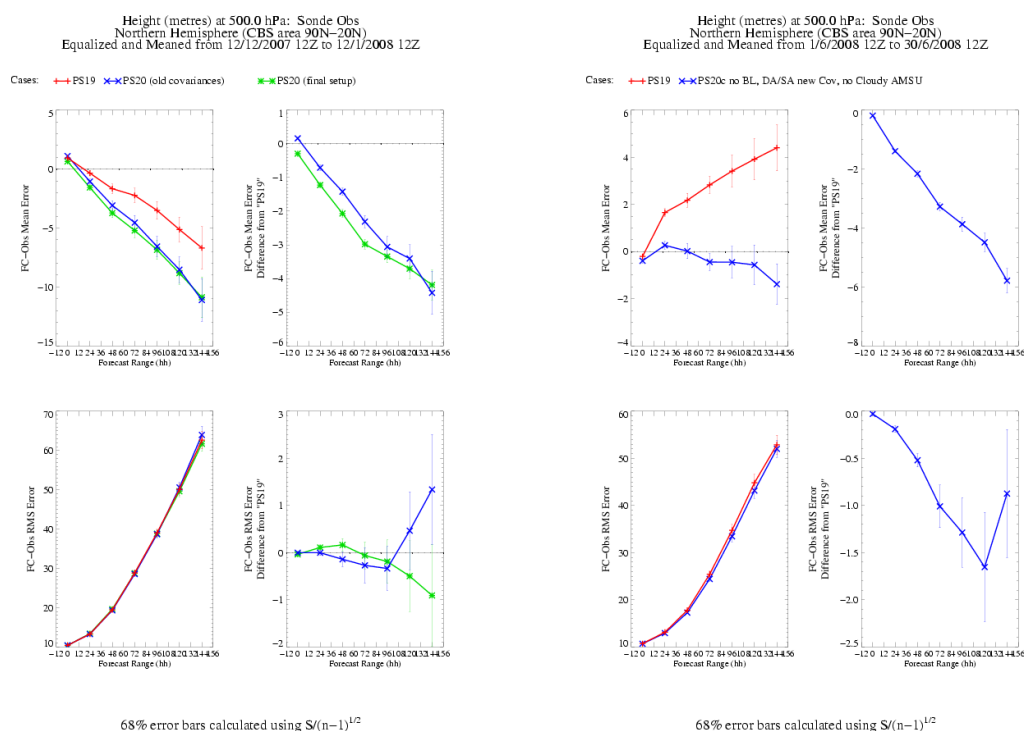


Figure 13: Impact of radiation changes to the G49 (PS20) package on NH 500hPa height forecasts for the December 2007 and June 2008 periods, verified against Sonde observations and compared to the previous G48 (PS19) model. The December trial also includes a version of the package without the new covariances described in Section 3.1.2.

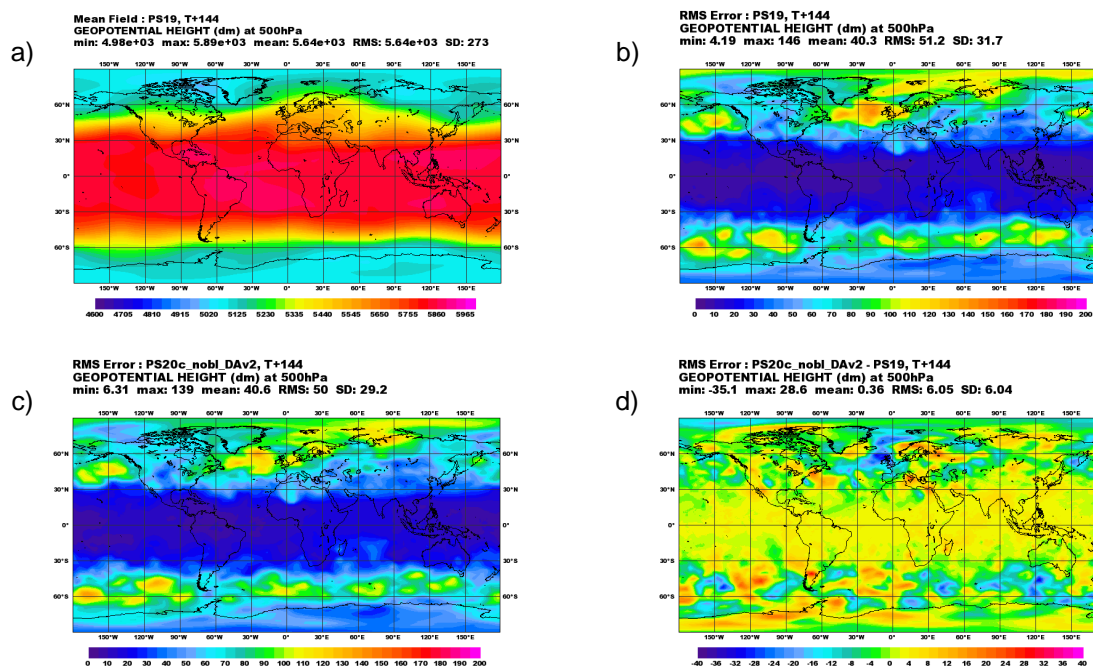
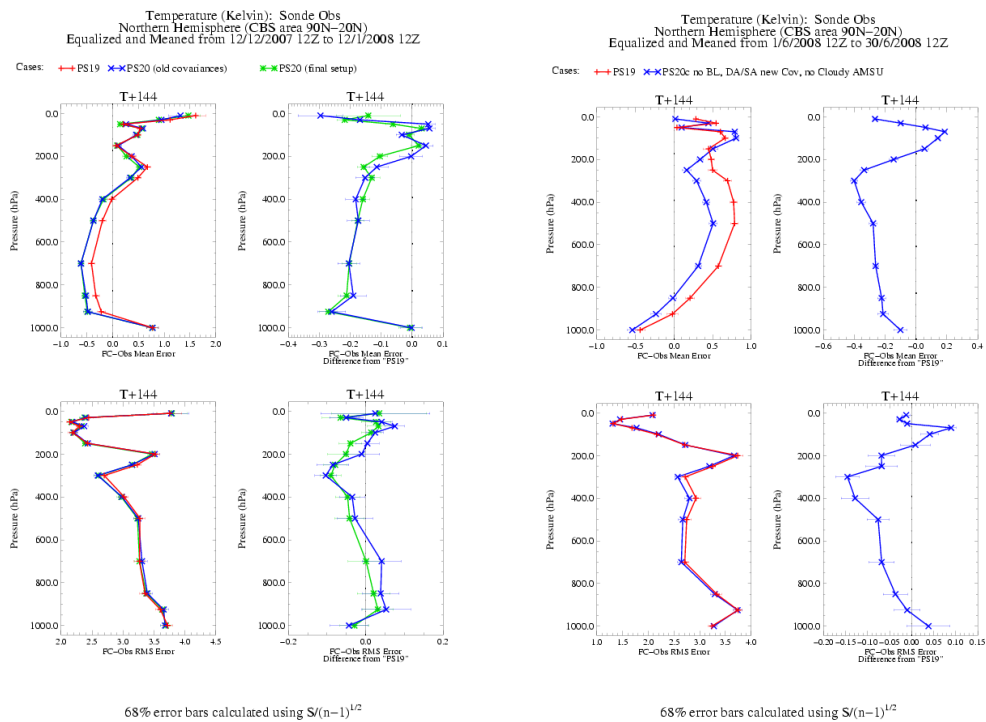


Figure 14: a) Mean 500hPa height analyses (which verify at the same times as panels b-d), during the December Trial from the PS19 control analyses, for reference against the forecast RMS errors, at T+144, of the PS19 (b) and PS20 (c) trials, and their differences (d).



X

Figure 15: Impact of radiation changes to the G49 (PS20) package on NH temperature profile forecasts at T+144 for the December 2007 and June 2008 periods, verified against Sonde observations and compared to the previous G48 (PS19) model. The December trial also includes a version of the package without the new covariances described in Section 3.1.2.

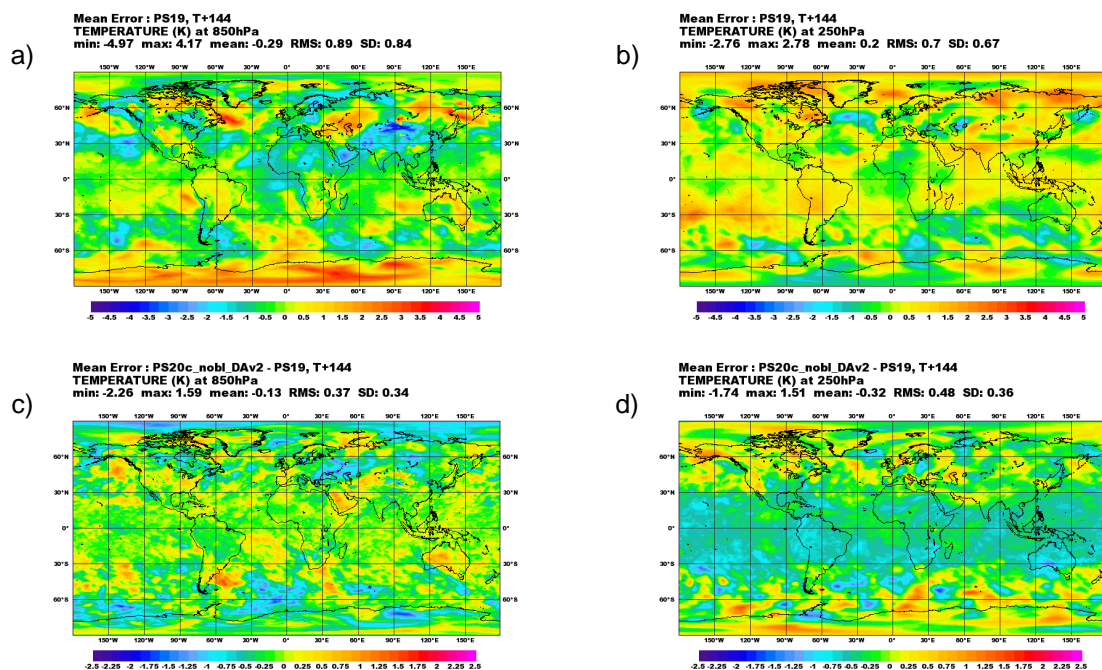


Figure 16: Mean temperature biases against analyses at T+144 from the December 2007 PS19 trial at a) 850hPa and b) 250hPa and the associated change in temperatures between the PS19 and PS20 configurations at c) 850hPa and d) 250hPa.

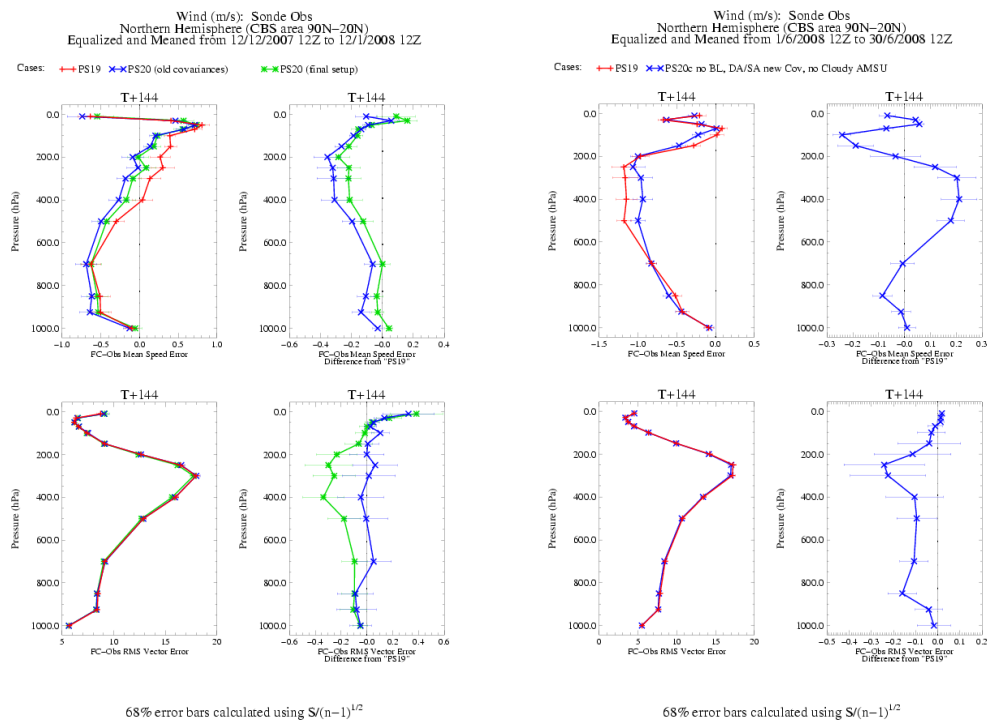


Figure 17: Impact of radiation changes to the G49 (PS20) package on NH wind speed profile forecasts at T+144 for the December 2007 and June 2008 periods, verified against Sonde observations and compared to the previous G48 (PS19) model. The December trial also includes a version of the package without the new covariances described in Section 3.1.2.

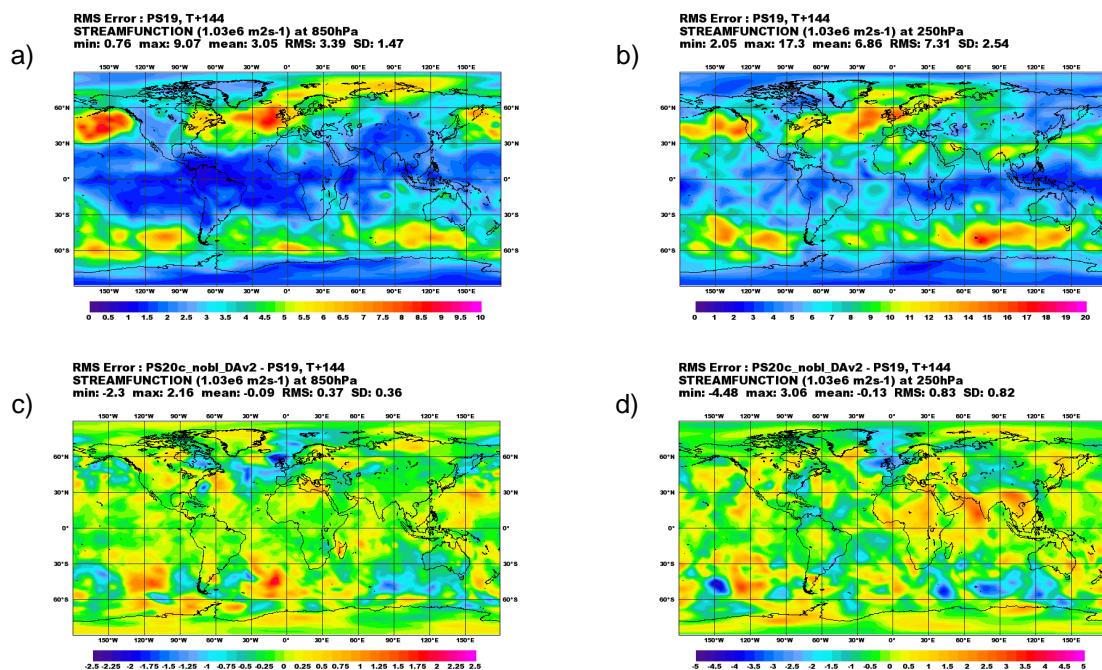


Figure 18: RMS errors of Streamfunction against analyses at T+144 from the December 2007 PS19 trial at a) 850hPa and b) 250hPa and the associated changes in RMS error between the PS19 and PS20 configurations at c) 850hPa and d) 250hPa.

to increase a cool bias from $\sim -0.3\text{K}$ to -0.5K , while in Summer a warm bias is reduced from $\sim +0.7\text{K}$ to $\sim +0.3\text{K}$. The centring of the Summer and Winter biases round 0 is a desirable for an operational weather prediction model. The maps of the change in the temperature bias, against analyses for the December trial, are shown in Figure 16. The temperature change at low levels (850hPa) is mostly in the Extra-Tropics and is co-located with regions of High pressure (see Figure 12), where clear skies are most likely. This indicates that this is caused by the change in the Rayleigh scattering properties of dry air which is shown to cause a cooling in Figure 8. At higher levels (at 250hPa), there is widespread cooling associated with the change to more realistic optical properties of ice clouds (again see Figure 8). The impact of the change in the optical properties of cirrus is shown to be beneficial in comparison to sonde observations in Figure 19 where the PS20 package appears to be correcting a warm bias and reducing the RMS error in both seasons.

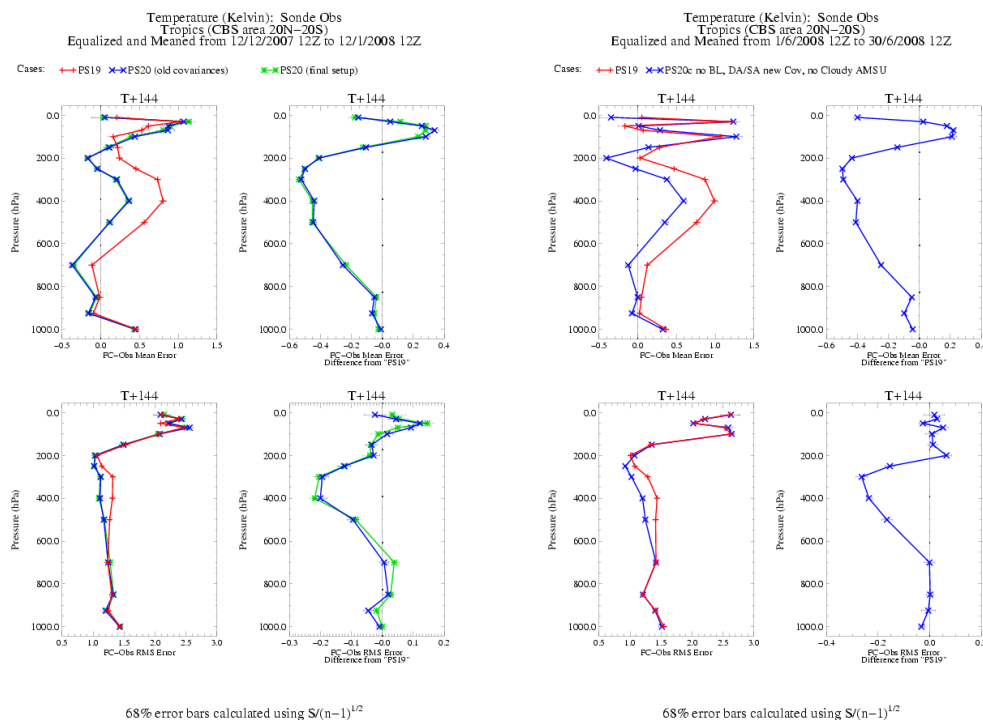


Figure 19: Impact of radiation changes to the G49 (PS20) package on Tropical temperature profile forecasts at T+144 for the December 2007 and June 2008 periods, verified against Sonde observations and compared to the previous G48 (PS19) model. The December trial also includes a version of the package without the new covariances described in Section 3.1.2.

The impact of the PS20 package on wind speed forecasts is shown in Figure 17, which shows an improvement in the RMS errors against sonde observations in both seasons, while upper level positive and negative biases are both reduced in Winter and Summer respectively. Again, the reduction in RMS error is much less in the trial without the new covariance statistics. The RMS errors of the forecast 850 and 250hPa streamfunction, against analyses, at T+144, are shown in Figure 18

for the PS19 configuration and the change due to the PS20 upgrade, for December 2007. An error in the streamfunction indicates a misplacement of the large scale cyclonic/anti-cyclonic circulations. The streamfunction RMS errors are clearly largest in the storm track regions, and these areas are significantly improved by the PS20 upgrade.

4.2 Global NWP Index Impact

Within the Met Office the performance of the global model in forecasting the global large scale circulation is often measured using a metric known as the Global NWP index. This index is defined as the weighted average of a basket of skill scores (SS) comparing the RMS errors of the forecast field (r_f) and the RMS error a persistence forecast (r_p),

$$SS = 1 - \frac{r_f^2}{r_p^2}, \quad (1)$$

where the persistence forecast is obtained by maintaining the model initial conditions throughout the forecast period. Such a skill score highlights the model's ability to forecast changeable conditions (Extra-Tropical cyclones etc) but makes it difficult for the model to demonstrate skill during static conditions (e.g. blocking high pressure systems). The SS is calculated for a number of parameters and forecast lead times and weighted to reflect the importance of the global model parameters to Met Office customers (highlighting long range forecasting over the UK and aviation forecasts), as shown in Table 4. The operational Global NWP index is a 3-year running mean of the weighted skill scores against observations and analyses, while trials are assessed by computing the change in the weighted NWP index.

		Forecast Range				
		T+24	T+48	T+72	T+96	T+120
NH	P_{msl}	10	8	6	4	4
	H_{500}	6	4	2	0	0
	W_{250}	12	0	0	0	0
Tropics	W_{850}	5	3	2	0	0
	W_{250}	6	0	0	0	0
SH	P_{msl}	5	4	3	2	2
	H_{500}	3	2	1	0	0
	W_{250}	6	0	0	0	0

Table 4: Parameters used for the calculation of the global NWP index, and their weights. Abbreviations refer to Northern and Southern Hemispheres (NH, SH) and Pressure at Mean Sea Level (P_{msl}), Heights (H) of the 500hPa pressure surface and Winds (W) at different pressure levels.

The Global NWP index impact of the PS20 package, shown in Table 5 for the different PS20 trials, highlights the strong overall performance of the package, particularly for the comparison against analyses, which was positive in all three trials, while the index against observations is positive in 2

out of 3 trials. Treating all 3 trials as equal, the average NWP index improvement is $\sim +1.6$, which makes up a significant proportion of the 2.3 increase specified as the Met Office's forecast accuracy key performance target for the 2008-9 financial year.

Trial Period	NWP Index vs Observations	NWP Index vs Analyses
Trial, Dec 07:	-0.864(-0.655%)	+2.805(+1.955%)
Trial, Jun 08:	+0.636(+0.515%)	+2.103(+1.587%)
PS20 itself:	+1.233(+0.879%)	+4.105(+2.741%)

Table 5: Impact on the Global NWP index in the Package Trials and Parallel Suite 20 (October-November 2008)

4.3 UK Index Impact

Within the Met Office the performance of the NAE model in forecasting surface weather parameters is often measured using a metric known as the U.K index. This index is defined as the weighted average of a basket of parameters as detailed in Table 6.

		Forecast Range							
		T+6	T+12	T+18	T+24	T+30	T+36	T+42	T+48
Surface Visibility <i>ETS</i>	200m	2	2	2	2	2	2	2	2
	1000m	2	2	2	2	2	2	2	2
	4000m	2	2	2	2	2	2	2	2
6 hr Precip Accum <i>ETS</i>	0.2mm	2	2	2	2	2	2	2	2
	1.0mm	2	2	2	2	2	2	2	2
	4.0mm	2	2	2	2	2	2	2	2
Total Cloud Amount <i>ETS</i>	0.31	1	1	1	1	1	1	1	1
	0.56	1	1	1	1	1	1	1	1
	0.81	1	1	1	1	1	1	1	1
Cloud Based Height (3/8 Cover) <i>ETS</i>	100	1	1	1	1	1	1	1	1
	500	1	1	1	1	1	1	1	1
	1000	1	1	1	1	1	1	1	1
Temperature <i>SS</i>	Screen	6	6	6	6	6	6	6	6
Wind <i>SS</i>	10m	6	6	6	6	6	6	6	6

Table 6: Parameters used for the calculation of the UK index and their weights. The *ETS* is the Equitable Threat Score and the *SS* is defined in equation 1.

The UK index impact of the PS20 package, shown in Figure 20 shows that there was an improvement to the *ETS* skill score for all variables and for all verification areas. The *ETS* skill score measures the fraction of observed events that were correctly predicted reduced by the fraction expected to be predicted by random chance (Schaefer (1990)). The *ETS* ranges from $-\frac{1}{3}$ to 1, with 1 indicating a perfect forecast and 0 indicating that the system has no skill. Over the larger verification areas, the largest *ETS* improvements were to precipitation and cloud cover. Over the UK, the precipitation *ETS* still showed a large improvement whilst cloud cover showed a neutral signal. The visibility scores over the UK were volatile, with a large difference in *ETS* improvement between Areas 2103 and 2014 (which only differ in the inclusion of Republic of Ireland stations in WMO Block 03 stations).

Parameter	Control Data	Test Data	Test - Control
	Mean ETS	Mean ETS	Wted ETS Diff
Surface Visibility	0.158	0.161	0.045
6 hr Precip Accum	0.348	0.355	0.138
Total Cloud Amount	0.334	0.350	0.161
Cloud Based Height (3/8 Cover)	0.246	0.252	0.066
	Mean Skill	Mean Skill	Wted Skill Diff
Surface Temp	0.742	0.744	0.025
Surface Wind	0.724	0.726	0.033

Total Weighted Score (%)
Control Case = 45.257
Test Case = 45.725
Test - Control = 0.468 (1.03 % change)

Parameter	Control Data	Test Data	Test - Control
	Mean ETS	Mean ETS	Wted ETS Diff
Surface Visibility	0.118	0.118	0.001
6 hr Precip Accum	0.304	0.310	0.120
Total Cloud Amount	0.308	0.309	0.015
Cloud Based Height (3/8 Cover)	0.271	0.273	0.020
	Mean Skill	Mean Skill	Wted Skill Diff
Surface Temp	0.839	0.841	0.030
Surface Wind	0.775	0.775	0.002

Total Weighted Score (%)
Control Case = 46.494
Test Case = 46.682
Test - Control = 0.188 (0.40 % change)

Parameter	Control Data	Test Data	Test - Control
	Mean ETS	Mean ETS	Wted ETS Diff
Surface Visibility	0.151	0.154	0.067
6 hr Precip Accum	0.358	0.366	0.162
Total Cloud Amount	0.299	0.316	0.170
Cloud Based Height (3/8 Cover)	0.265	0.268	0.037
	Mean Skill	Mean Skill	Wted Skill Diff
Surface Temp	0.797	0.799	0.024
Surface Wind	0.773	0.775	0.049

Total Weighted Score (%)
Control Case = 47.210
Test Case = 47.720
Test - Control = 0.509 (1.08 % change)

Parameter	Control Data	Test Data	Test - Control
	Mean ETS	Mean ETS	Wted ETS Diff
Surface Visibility	0.107	0.113	0.117
6 hr Precip Accum	0.300	0.306	0.134
Total Cloud Amount	0.313	0.313	0.001
Cloud Based Height (3/8 Cover)	0.274	0.276	0.021
	Mean Skill	Mean Skill	Wted Skill Diff
Surface Temp	0.841	0.842	0.034
Surface Wind	0.776	0.776	0.008

Total Weighted Score (%)
Control Case = 46.325
Test Case = 46.640
Test - Control = 0.315 (0.68 % change)

Figure 20: Impact of PS20 on UK Index scores. The figure shows results for Area 514 [Reduced NAE model Area] (top left), Area 503 [Mesoscale Model Area] (top right), 2103 [Block 03 Stations Area](bottom left) and 2014 [UK Index Stations Area](bottom right).

4.4 Surface variables

The impact of PS20 changes on the NAE model resulted in a systematic cooling of screen temperatures throughout the diurnal cycle. This reduced the warm bias seen at 00Z 06Z and 18Z and worsened the cold bias at 12Z (Figure 21). The NAE warm bias seen at 00Z and 06Z is quite persistent throughout the year whilst the warm bias at 18Z changes to a cold bias in the Winter season.

The screen relative humidity dry bias is slightly improved in the NAE and slightly worsened in the Global model (Figure 22). The sign of the frequency bias for the 200m visibility threshold (fog) is changed in the NAE (Figure 23). Prior to PS20, the model under-forecast fog whilst the PS20 NAE forecasts too much. Looking at the 1000m and 4000m visibility thresholds, one can see that PS20 forecasting more aviation fog and mist events and this improves the previous under-forecasting of these events. In a similar manner to the global model circulation forecasts described in Section 4.1, the negative P_{msl} bias and positive wind speed bias in the NAE model are both improved by the PS20 package (see Figures 24 and 25).

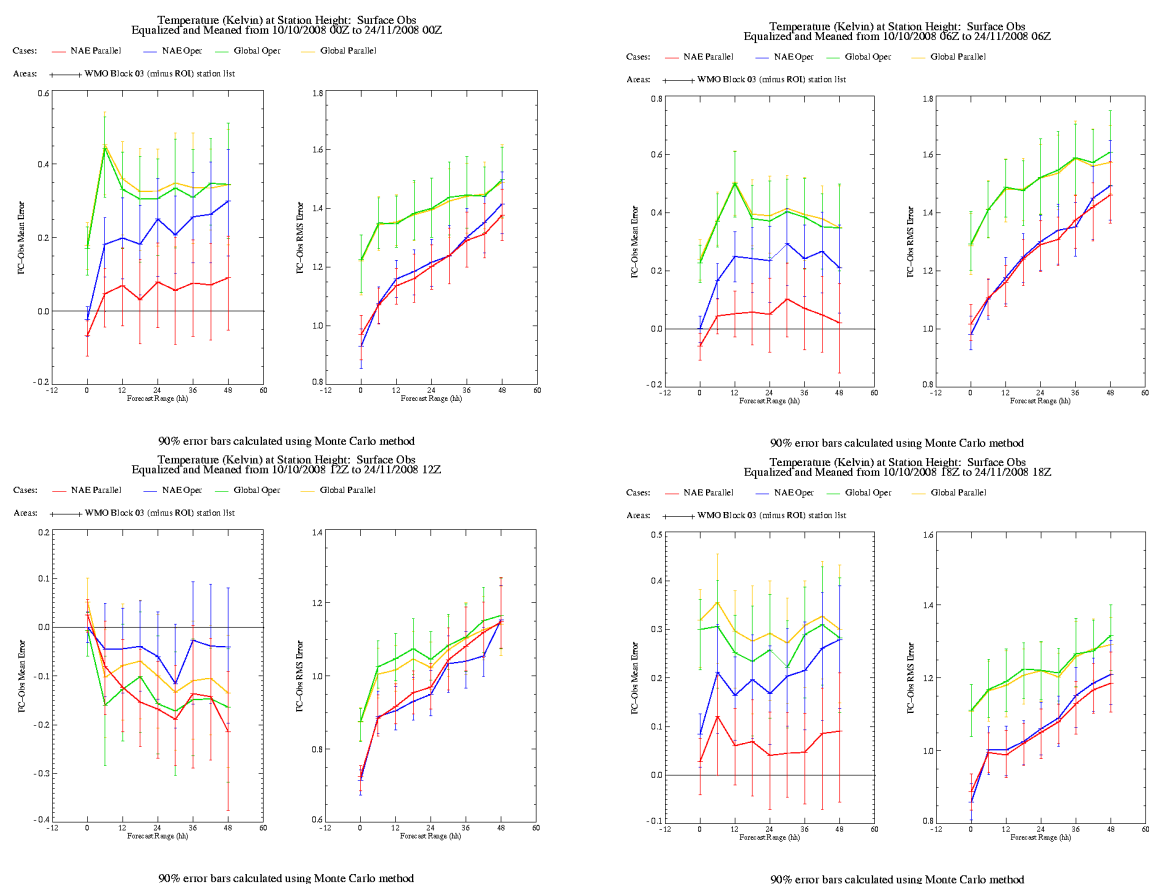


Figure 21: Impact of PS20 on screen temperature errors through the diurnal cycle. The figure shows bias and RMSE for both NAE and Global models as a function of forecast range, at 00Z (top left), 06Z (top right), 12Z (bottom left) and 18Z (bottom right).

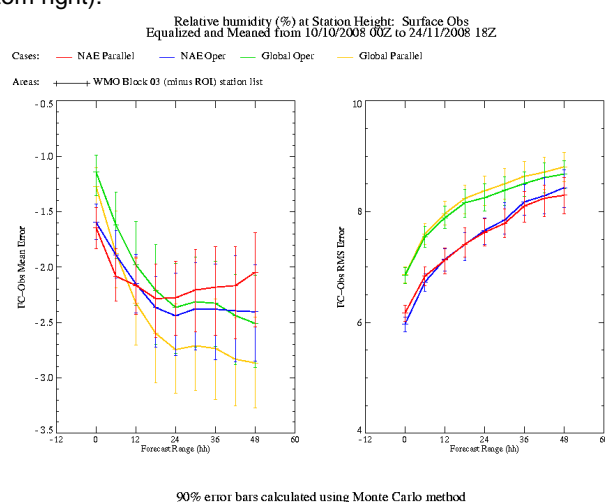


Figure 22: Impact of PS20 on screen relative humidity. The figure shows bias and RMSE for both NAE and Global models as a function of forecast range.

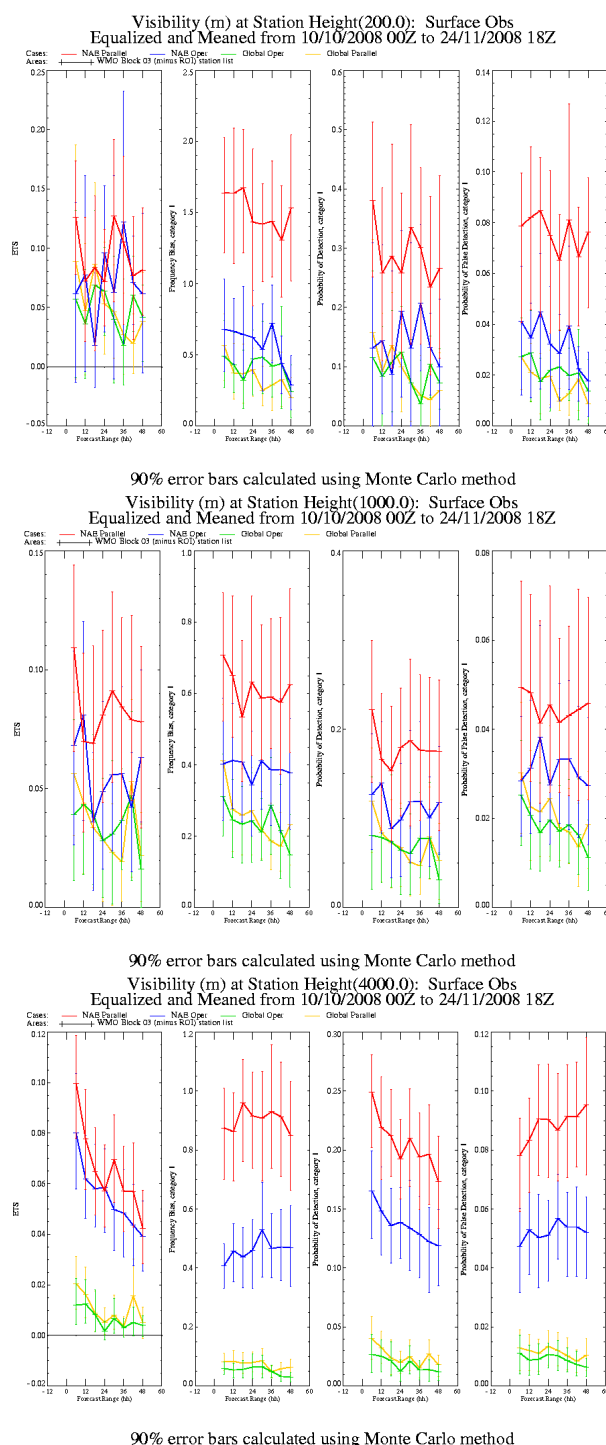


Figure 23: Impact of PS20 on screen visibility at the 200m (top) 1000m (middle) and 4000m (bottom) thresholds. The panels in the figure show ETS, frequency bias, probability of detection and probability of false detection for both NAE and Global models as a function of forecast range.

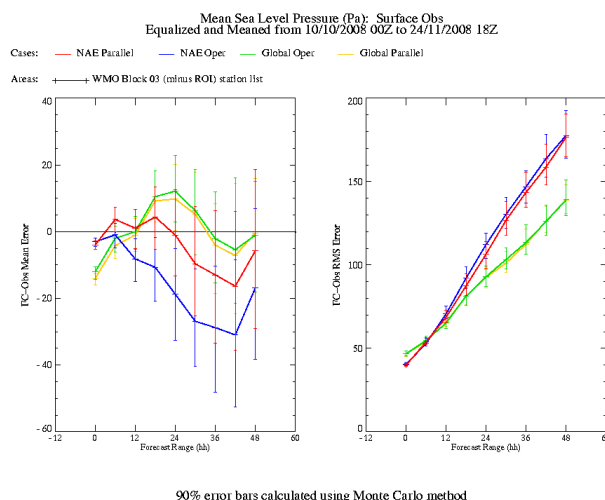


Figure 24: Impact of PS20 on PMSL. The figure shows bias and RMSE for both NAE and Global models as a function of forecast range.

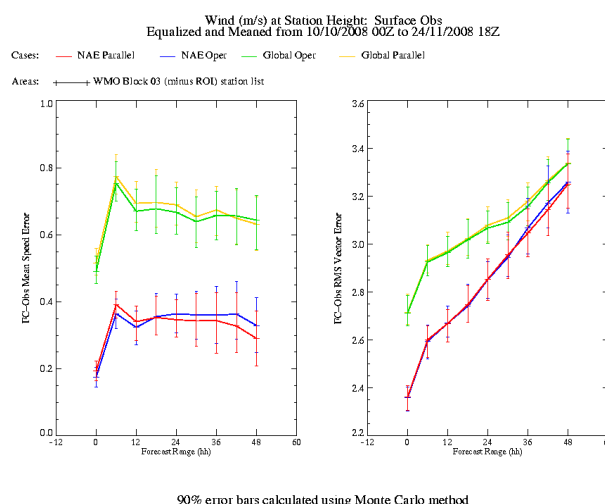


Figure 25: Impact of PS20 on 10m wind. The figure shows bias and RMSE for both NAE and Global models as a function of forecast range.

4.5 Cloud and precipitation

The negative cloud cover bias is slightly worsened in both the NAE and Global models (Figure 26). The NAE case studies showed that a large part of this change was caused by the radiation changes (Figure 9). The change in the frequency bias scores indicates that the amount of drizzle is slightly reduced in both the NAE and Global models, due to change from 3C to 3D microphysics and the linking of MURK aerosol to autoconversion in the NAE (Figure 27). Both the PS20 configurations of the Global and NAE models showed an increase in the *ETS* skill score for drizzle, especially at longer forecast lead times.

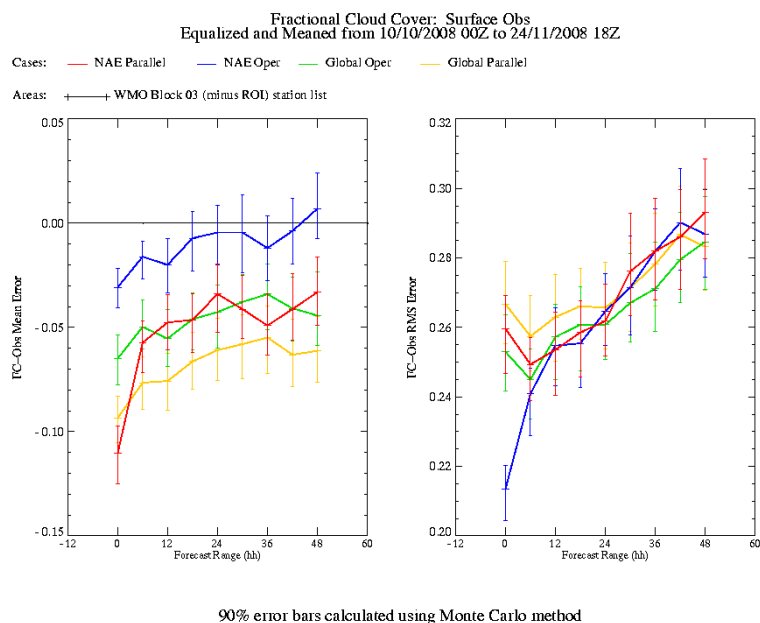


Figure 26: Impact of PS20 on cloud cover. The figure shows bias and RMSE for both NAE and Global models as a function of forecast range.

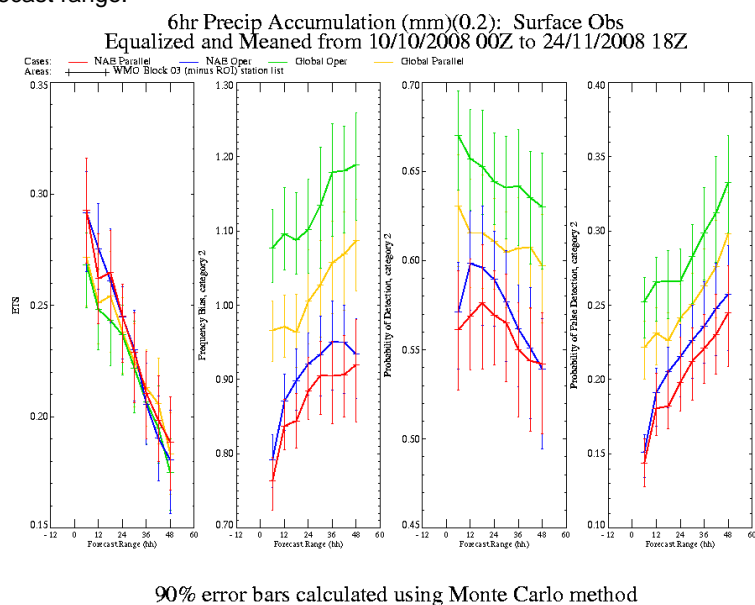


Figure 27: Impact of PS20 on drizzle (0.2mm precipitation accumulation in 6 hours). The figure shows ETS, frequency bias, probability of detection and probability of false detection for both NAE and Global models as a function of forecast range.

5 Conclusions

PS20 was implemented operationally on 25th November 2008, but an emergency change was made to the NAE model on 19th December 2008 to disable the MURK Link to Autoconversion, following a succession of excessive low visibility/thick fog events. Although these changes improved the *ETS* scores, the changes in the frequency bias discussed in 4.4 degraded the model's visibility forecasts utility for the forecasters. Subsequent reanalysis indicates that the MURK link to autoconversion can actually improve these events, with amended droplet numbers which will allow both rain-out of MURK and, in particular, reduction of BL moisture.

The PS20 package of changes were significantly beneficial to the performance of the global model in forecasting the large scale global circulation, with improvements in the RMS errors in related diagnostics (surface pressure, geopotential height, wind speed, streamfunction). These RMS errors were primarily reduced by improvements to the initial conditions of the forecast created by the data assimilation system. A number of changes to the radiation scheme and microphysics schemes were also introduced which improved the representation of the thermal structure of the atmosphere, notably reducing the temperature biases associated with tropical convection. The Global NWP index (a metric used within the Met Office to measure the performance of the global model in this respect) increased significantly against analyses in all trials (ranging from $\sim +2$ to $\sim +4$) and increased in 2 out of 3 trials against observations (ranging from ~ -1 to $\sim +1$). The magnitude of these changes was such that it provided the majority of the forecast accuracy improvements required to satisfy the Met Office's relevant key performance target for the year.

The performance of the NAE PS20 package was examined against diagnostics more associated with the local weather: screen temperature, 10m wind, cloud, precipitation and visibility. There was an improvement to the *ETS* for all variables and for all verification areas. Measured verification plots revealed that the improved visibility *ETS* scores were accompanied by significant improvements to the bias. The PS20 NAE does forecast too much thick fog, although the increase in aviation fog and mist at the 1000m and 4000m thresholds improves the previous under-forecasting of these events. The improved precipitation scores are due to reduced frequency biases particularly for drizzle and light rain, leading to reduced probabilities of false detection.

Overall, the PS20 package of changes provided a significant improvement to the Met Office capability for Numerical Weather Prediction. Changes to the data assimilation system and representation of the model physics led to an improvement of the skill of forecasting the large scale atmospheric circulation, particularly at longer time ranges. The surface 'weather' variables were improved directly at all time ranges through the model physics changes, and at longer time scales through the improvements to the large scale circulation. The adoption of a common version of the Met Office

Unified Model code (MetUM, vn7.1), was vital for the implementation of the forecast suite on the IBM supercomputer and assisted in the convergence of the remaining differences between the Met Office global NWP and climate models.

References

- Abel, S. J. and Shipway, B. (2007). A comparison of cloud resolving model simulations of trade wind cumulus with aircraft observations taken during RICO. *Quart. J. Roy. Meteor. Soc.*, **133**(624), 781–794.
- Bettenhausen, M., Smith, C., Bevilacqua, R., Wang, N., Gaiser, P., and Cox, S. (2006). A nonlinear optimization algorithm for windsat wind vector retrievals. *IEEE Trans. on Geosci. and Rem. Sens.*, **44**(3), 597–609.
- Brooks, M. E. and Jones, C. (2007). Initial evaluation of the classic modis albedo product for use in operational nwp. Met Office internal link: http://www-nwp/freb/SWANSEA.MODIS.ALBS/Swansea_albedos_v2_CAP.ps.gz.
- Brown, P. R. A. and Francis, P. N. (1995). Improved measurements of the ice water content in cirrus using a total water probe. *J. Atmos. Oceanic Technol.*, **12**, 410–414.
- Candy, B., Atkinson, N., and English, S. (2008). Does the atovs rars network matter for global nwp? In *In Proc. of the 16th International TOVS Study Conference, Angra dos Reis, Brazil*.
- Candy, B., English, S., and Keogh, S. (2009). A comparison of the impact of quikscat and windsat wind vector products on met office analyses and forecasts. *IEEE Trans. on Geosci. and Rem. Sens.*, **47**(6), 1632–1640.
- Clark, P. A., Harcourt, S. A., Macpherson, B., Mathison, C. T., Cusack, S., and Naylor, M. (2008). Prediction of visibility and aerosol within the operational Met Office Unified Model. i: Model formulation and variational assimilation. *Q. J. Roy. Met. Soc.*, **134**, 1801–1816.
- Edwards, J., Havemann, S., Thelen, J.-C., and Baran, A. (2007). A new parametrization for the radiative properties of ice crystals: Comparison with existing schemes and impact in a gcm. *J. of Atmos Research*, **83**, 19–35.
- Essery, R., Martin, E., Douville, H., Fernandez, A., and Brun, E. (1999). A comparison of four snow models using observations from an alpine site. *Clim. Dyn.*, **15**, 583–593.
- Haywood, J. M., Bush, M., Osborne, S., Abel, S. J., Claxton, B., Macpherson, B., Harrison, M., Crosier, J., and Coe, H. (2008). Prediction of visibility and aerosol within the operational met office unified model. part 1: validation of model performance using observational data. *Quart. J. Roy. Meteor. Soc.*, **134**, 1817–1832. doi: 10.1002/qj.275.

- Helfrich, S., McNamara, D., Ramsay, B. H., Baldwin, T., and Kasheta, T. (2007). Enhancements to, and forthcoming developments in the interactive multisensor snow and ice mapping system (*ims*). *Hydrol. Proc.*, **21**, 1576–1586.
- Houldcroft, C., Grey, W., Barnsley, M., Taylor, C., Los, S., and North, P. (2008). New vegetation albedo parameters and global fields of background albedo derived from MODIS for use in a climate model. *J. Hydrometeorology*, **10**(1).
- Illingworth, A., Hogan, R. J., O'Connor, E., Brooks, M., Delanoe, J., Donovan, D., Gaussiat, N., Goddard, J., Haefflin, M., Baltink, H. K., Krasnov, O. A., Pelon, J., Piriou, J.-M., Protat, A., Russchenberg, H., Seifert, A., Tompkins, A., van Zadelhoff, G.-J., Vinit, F., Willen, U., Wilson, D. R., and Wrench, C. (2007). Cloudnet - continuous evaluation of cloud profiles in seven operational models using ground-based observations. *Bull. Amer. Meteor. Soc.*, **88**(6), 883–898. doi:10.1175/BAMS-88-6-883.
- Mercado, L. M., Huntingford, C., Gash, J. H. C., Cox, P. M., and Jogireddy, V. (2007). Improving the representation of radiation interception and photosynthesis for climate model applications. *Tellus B*, **59**(3), 553–565.
- Mitchell, D. L. (1996). Use of mass- and area-dimensional power laws for determining precipitation particle terminal velocities. *J. Atmos. Sci.*, **53**(12), 1710–1722.
- Moody, E., King, M., Platnick, S., Schaaf, C., and Feng, G. (2005). Spatially complete global spectral surface albedos: value-added datasets derived from terra modis land products. *IEEE Trans. on Geosci. and Rem. Sens.*, **43**, 144–158.
- Pope, V., Gallani, M., Rowntree, P., and Stratton, R. (2000). The impact of new physical parameterisations in the hadley centre climate model: Hadam3. *Clim. Dyn.*, **16**, 123–146.
- Pullen, S., Jones, C., and Rooney, G. (2008). Implementation of a northern hemisphere snow analysis in the global model. Met R&D Technical Note 526, Met Office, Met Office, FitzRoy Road, Exeter, EX1 3PB, <http://www.metoffice.gov.uk/research/publications>.
- Schaefer, J. T. (1990). The critical success index as an indicator of warning skill. *Weather Forecasting*, **5**, 570–575.
- Sellers, P., Berry, J., Collatz, G., Field, C., and Hall, F. (1992). Canopy reflectance, photosynthesis and transpiration iii. a reanalysis using improved leaf models and new canopy integration scheme. *Remote Sens. Environ.*, **42**, 187–216.

Met Office

FitzRoy Road, Exeter
Devon, EX1 3PB
UK

Tel: 0870 900 0100

Fax: 0870 900 5050

enquiries@metoffice.gov.uk

www.metoffice.gov.uk